

FILE COPY

ESD-TR 68-251

ESLE

AMPEX

ESD RECORD COPY

RETURN TO
SCIENTIFIC & TECHNICAL INFORMATION DIVISION
(ESTI), BUILDING 1211

ESD ACCESSION LIST.

ESTI Call No. 63281

Copy No. 1 of 1 c/s.

MICROWAVE FERRITE PROGRAM

RR 68-21

23 August 1968

RECEIVED

ESTI

DISTRIBUTION

Ampex Corporation
Research and Advanced Technology Division

AD678955

ESD-TR-68-251

FILE COPY

23 August 1968

Summary Technical Report
MICROWAVE FERRITE PROGRAM
Period Ending July 31, 1968

Paul D. Baba
Head, Ferrite Research Group

S. K. Banerjee
Member of the Research Staff

Prepared by
AMPEX Corporation
Redwood City, California

for
Massachusetts Institute of Technology
Lincoln Laboratory

This document has been approved for public
release and sale; its distribution is unlimited.

ABSTRACT

A program is described in which the objective was the development of a series of lithium ferrites for latching microwave device applications. Two families of compositions were explored -- lithium-aluminum ferrites and lithium-titanium ferrites. Microwave, hysteresis loop, and microstructural properties were investigated as functions of compositions and processing parameters. The lithium-titanium ferrites were found to have better sintering performance relative to the lithium-aluminum ferrites, and are considered promising materials for the intended microwave applications.

ACKNOWLEDGEMENTS

The authors gratefully acknowledge the support and guidance of the Project Technical Monitor, D. H. Temme, and G. F. Dionne, both of the Lincoln Laboratory.

In addition, the many technical consultations with Prof. J. Smit, University of Southern California and Prof. R. White, Stanford University, were also very beneficial.

The authors are also indebted to L. L. Moultrie, and D. G. Smith, Ampex Corporation, for their efforts in the preparation of samples.

CONTENTS

		Page
1.0	INTRODUCTION	1
2.0	EXPERIMENTAL APPROACH	3
	2.1 Sample Preparation	3
	2.2 Measurement Techniques	4
3.0	LIST OF COMPOSITIONS	11
4.0	LITHIUM-ALUMINUM COMPOSITIONS	15
	4.1 Materials with $4\pi M_s \simeq 1800$ Gauss	15
	4.2 Materials with $4\pi M_s \simeq 800$ Gauss	22
	4.3 Magnetic and Dielectric Loss	26
	4.4 Conclusion	40
5.0	LITHIUM-TITANIUM FERRITES	43
	5.1 General	43
	5.2 Conclusion	62
6.0	REFERENCES	63

1.0 INTRODUCTION

In response to a Request for information (#11302), from Lincoln Laboratory, Massachusetts Institute of Technology, a detailed program was outlined by Ampex to develop a number of lithium ferrite compounds. It was desired that the ferrite materials exhibit hysteresis loop squareness, temperature stability, good microwave properties and selected values of saturation magnetization. It was the object of the work primarily to provide materials which would be useful in devices, but secondarily to study the general principles relating ferrite preparation technology with microwave properties.

The specific design goals were initially set forth as follows:

<u>Property</u>	<u>Requirement</u>
1) Saturation moment ($4\pi M_s$)	200 to 2000 gauss
2) Resonance linewidth (ΔH)/ $4\pi M_s$	Less than 0.3
3) Squareness (defined as the ratio of remanent magnetization (B_r) to the magnetization at five times the coercive force, H_c).	Greater than 0.8 A well-defined knee in the second and fourth quadrant is desirable.
4) Magnitude of the switching field to produce a stable remanent magnetization	Less than 10 oersteds

<u>Property</u>	<u>Requirement</u>
5) Coercive force (H_c)	Less than 2 oersteds
6) Curie temperature (T_c)	For $4\pi M_s = 200$ gauss, greater than 300°C For $4\pi M_s = 2000$ gauss, greater than 500°C
7) Spin wave linewidth (ΔH_k)	Greater than 20 oersteds
8) Dielectric loss tangent ($\tan \delta_\epsilon$)	less than 0.0005
9) Magnetostriction (λ_s)	Similar to or less than magnesium-manganese ferrites

2.0 EXPERIMENTAL APPROACH

2.1 Sample Preparation

The oxides used in the preparation of ferrites are reagent grade oxides, with the exception of iron (III) oxide. The iron (III) oxide is from C. K. Williams and is certified 99.3% pure. When the use of alkali oxides is necessary, carbonates of the alkali metals are selected as convenient weighable compounds. The alkali carbonate employed (lithium) is of reagent grade. Transition metal carbonates are frequently desirable starting materials when the particle size of their oxides is prohibitive.

After the oxides and carbonates are weighed they are placed in either a 1 liter or a 1-1/2 liter ball mill jar with 5/16 in. diameter stainless steel balls. Water is generally used as a mixing vehicle except when one or more of the constituent oxides or carbonates exhibit a water solubility, as is the case when lithium carbonate is present. A convenient substitute for water is isopropyl alcohol. The slurry obtained when the mixing is completed is then separated from the steel balls and dried. After drying, the material is given a preliminary heat treatment ("calcining") to remove gaseous products and to form the spinel structure. A second ball milling operation is used to crush the agglomerates formed by the reaction.

The reacted oxide mixture is dried after the ball milling operation and forced through a 20 mesh screen. A polyvinyl alcohol-water or isobutyl methacrylate-xylene suspension is then added, and the material is suitably granulated for pressing in a die.

The shape and size of samples pressed are shown in Fig. 1. A total force of 5000 pounds is used for cores and cylinders. Various forces were tried and 5000 pounds appeared to be optimum.

The sintering operation employed soak temperatures ranging from 1000° C to 1300° C in both air and oxygen atmospheres for periods of 3 to 20 hours.

2. 2 Measurement Techniques

2. 2. 1 Density

Densities were obtained from weight, diameter, and height measurements taken on cylinders which were approximately 0. 530 inch in diameter and between 0. 500 and 0. 600 inch in height.

2. 2. 2 Magnetic and Dielectric Losses

Magnetic and dielectric losses were measured in an S-band helical phase shifter [Ref. 1]. Figure 2 is a block diagram of the apparatus used. The oscillator produces square waves with 1 KHz modulation, which, after passing through the attenuator, enters the helical phase shifter. The db loss of signal on insertion of two ferrite cylinders is measured using the oscilloscope. Gd-doped garnets of comparable $4\pi M_s$ values were used as standards. A routine measurement of magnetic and dielectric losses consisted of the following steps:

1. Measure the reference power from the oscillator, bypassing the phase shifter.

2. Insert the phase shifter as shown in Fig. 2. The phase shifter contains a cylinder of microwave materials, either a ferrite or a garnet of comparable $4\pi M_s$ value. Note the loss of signal in db. This is termed the "total loss."

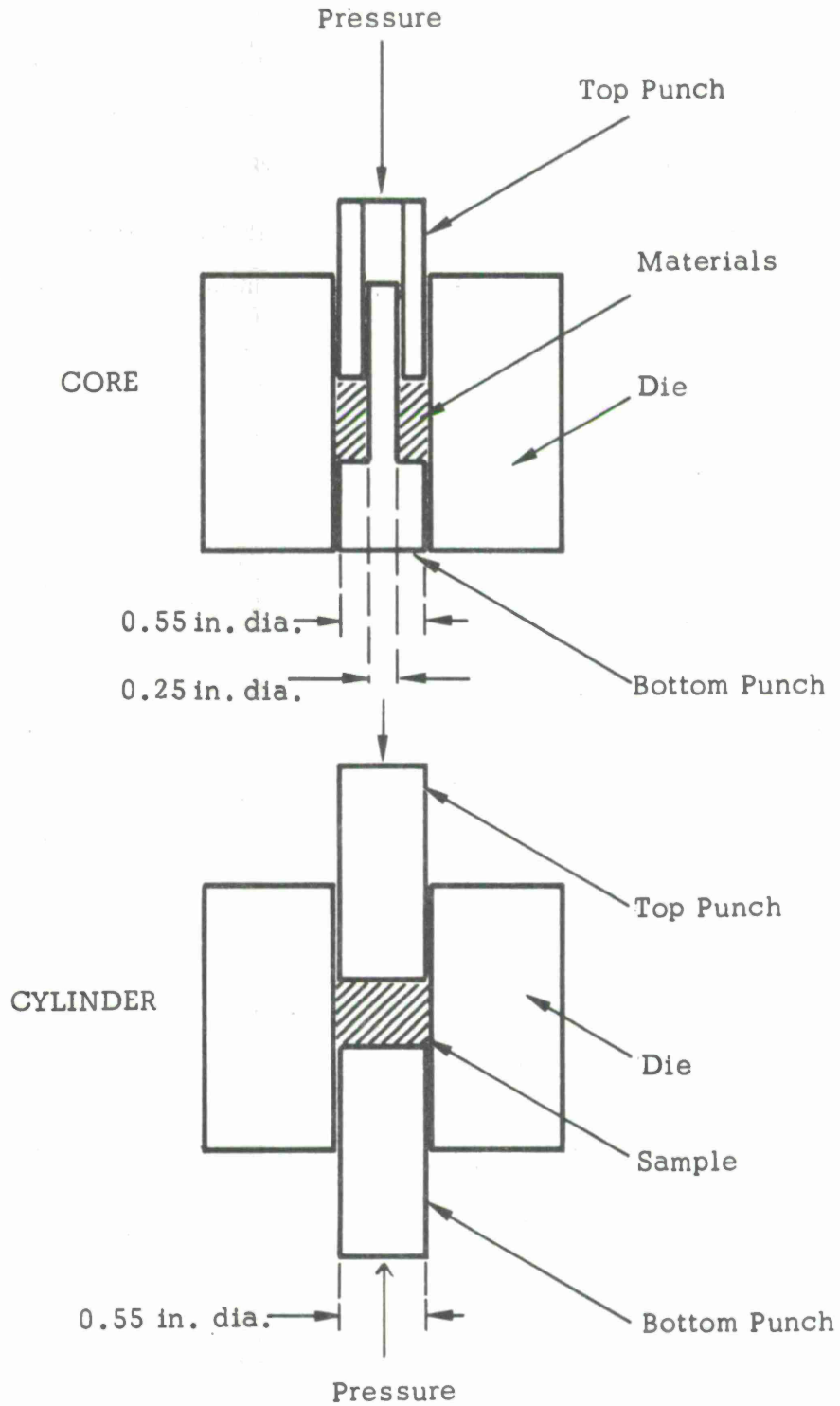


Fig. 1 Dies and Punches used for Forming "Green" Toroids and Cylinders

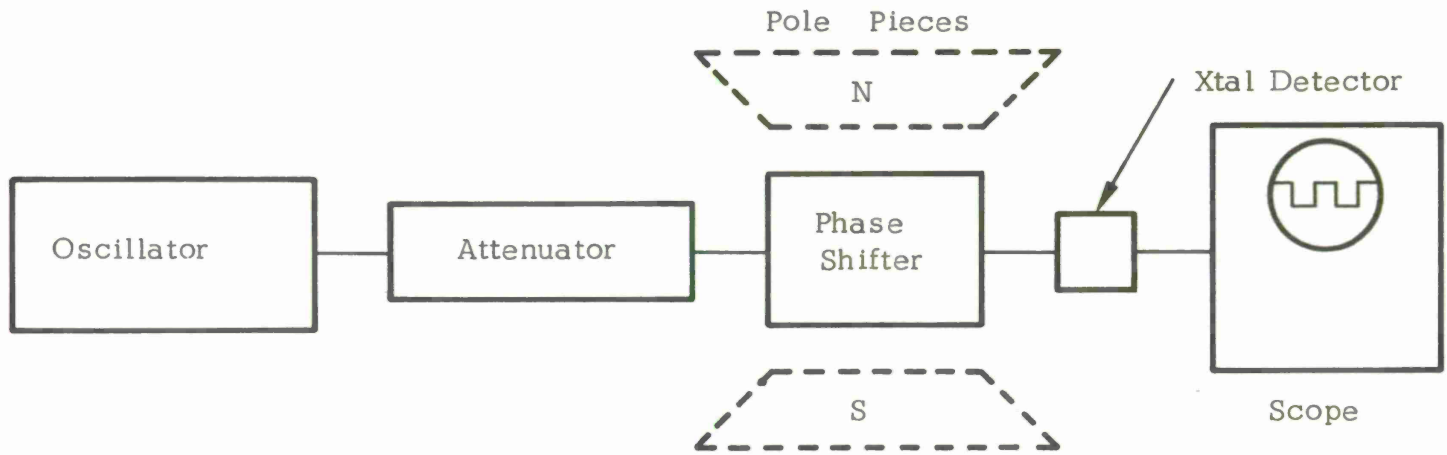


Fig. 2 Block Diagram for Loss Measurement

3. With the circuit as shown in Fig. 2 insert only the phase shifter between the pole pieces of an electromagnet. Increase the magnetic field to until the signal level is maximized and is constant. This happens around 2000 Oe, but to be absolutely sure, we used the value of 7000 Oe as the acceptable value. By comparing with the reference level, the db loss in the present configuration was obtained. This was termed the "dielectric loss." In the magnetically saturated state at 7000 Oe where no domain walls were present, the loss should primarily be due to dielectric losses plus the copper loss of the helical phase shifter.

4. The difference between the total and the dielectric losses was termed the "magnetic loss." This could be determined directly by comparing the signal levels when the ferrites (or garnets) were 1) in an unmagnetized state in zero applied field and 2) in a saturated state in 7000 Oe applied field.

For a regular check of the apparatus as a whole, the magnetic and dielectric losses of a pair of standard garnet samples were measured prior to the measurements on the experimental samples.

2. 2. 3 Saturation Magnetization and Curie Point

After the measurement of magnetic and dielectric losses, one of the two ferrite cylinders was stored and the other cut into slices, 1/8 in. thick. From the slices, two 1/8 in. cubes were prepared, which were then ground into spheres of 2.5 to 3.0 mm in diameter by tumbling in an air tumbler with abrasive lining. One of the spheres was stored for resonance linewidth measurement (to be described below) while the other was weighed to four decimal places and then mounted on a quartz rod with "Sauereisen" cement for the measurement of saturation magnetization and Curie point.

Saturation magnetization was measured using a "Foner type" vibrating sample magnetometer at room temperature (300° K) in a magnetic field of 10,000 Oe.

The Curie point was then determined for the above sphere by inserting a heater inside the vibrating sample magnetometer. The measuring field was 500 Oe in order to decrease the "tail" observed when measuring in high fields like 10,000 Oe. The "tail" is due to the presence of short range order above the Curie point and the absence of it makes the determination of Curie point easier. Both heating and cooling curves were obtained. Although they didn't overlap over the whole temperature range because of thermocouple lag, enough time was spent to let the sample regain room temperature. This procedure confirmed from the magnetization values before and after heating that the sample does not undergo a chemical change on heating to its Curie point. Figure 3 shows an example of Curie point determination for Sample #L-21-71/F576.

2.2.4 Resonance Linewidth

Routine measurements of ferrimagnetic resonance linewidth were carried out in accordance with the ASTM method [Ref. 2] using a transmission cavity resonating at 2.84 GHz.

2.2.5 Remanence and Coercive Force

For remanence ($4\pi M_r$) measurements, the previously mentioned toroids were used. Usually, 5 turns of wire were used for driving and 10 turns for sensing the flux. Hysteresis loops were obtained in the conventional manner by integrating the voltage output and displaying the integrated signal on an oscilloscope as a function of the driving current. For a check of the calibration, two standards were used: a garnet toroid with a coercive force of 1.2 Oe and a ferrite with a 6.3 Oe coercive force. Photographs were taken of the loops displayed on the oscilloscope. The toroids were driven to a maximum ac field which was equal to 3 times the coercive force.

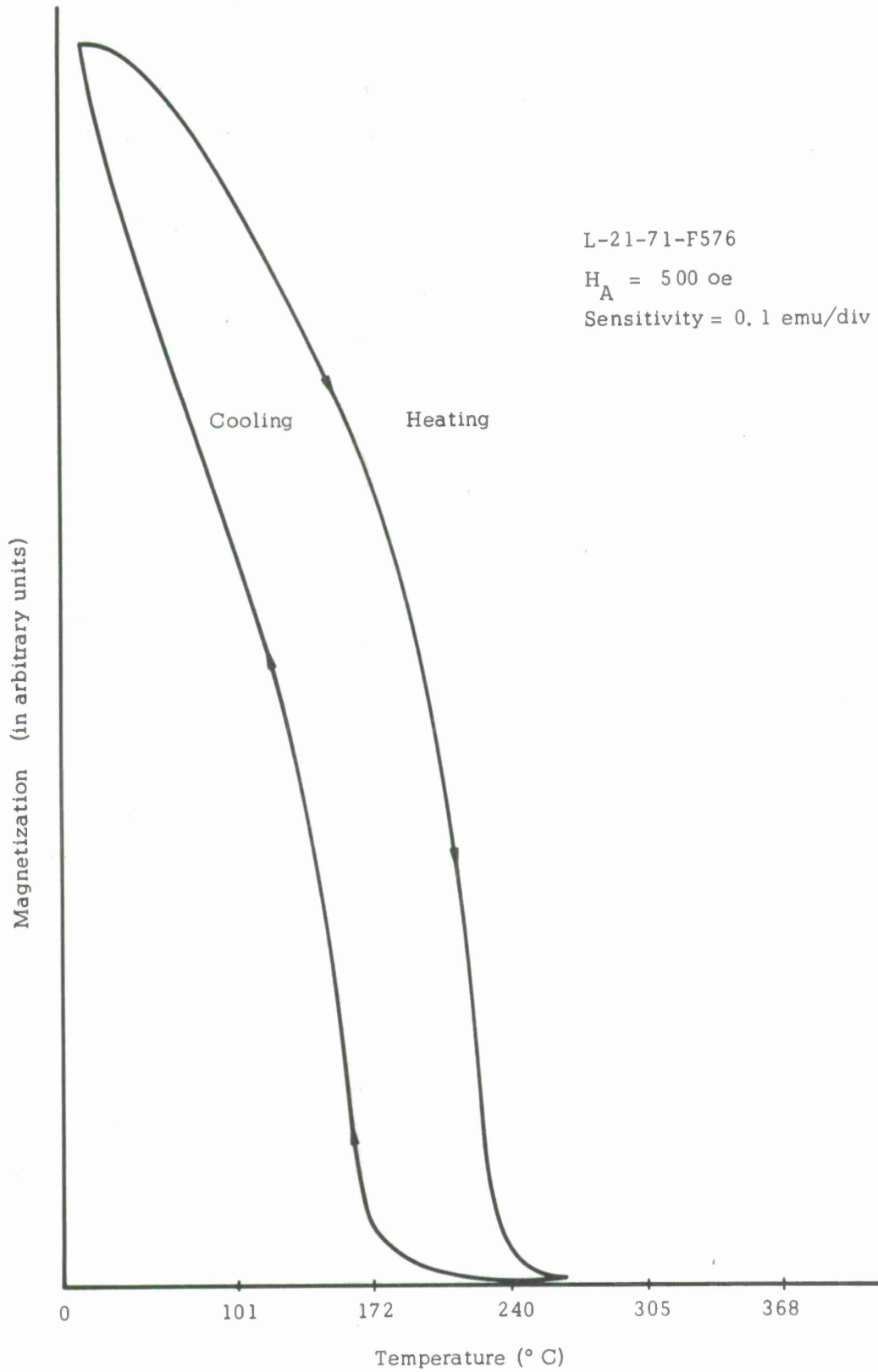


Fig. 3 Example of Curie Point Determination

Toroids were occasionally sliced up to make into spheres for $4\pi M_s$ measurements. It was found that these $4\pi M_s$ values were not significantly different if spheres from a cylinder of the same chemical composition were used. This shows that although our B_r and $4\pi M_s$ values were obtained from different samples, the remanence ratios $B_r/4\pi M_s$ are reliable.

Temperature variation of B_r was studied for selected samples by dipping the toroids into a constant temperature (70° C) bath filled with a nonconducting oil.

2. 2. 6 Resistivity

Direct current (dc) resistivities were obtained from the ferrite cylinders. The two ends were coated with indium amalgam and then placed between copper electrodes under a slight pressure. The resistance (R) in ohms was measured using a megohm-meter, and the resistivity was calculated.

2. 2. 7 Microstructure

Microstructural observations were carried out on polished and etched slices of the ferrites. The samples were etched either chemically, using hot mixtures of oxalic and sulphuric acid, or thermally. The optically observed microstructure was correlated with the calculated density.

2. 2. 8 Mossbauer Spectra

Selected samples were used in Mossbauer effect measurements to confirm the cation distribution as concluded from saturation magnetization measurements at 77° K. The Mossbauer work was carried out at various temperatures between 4. 2° K and 950° K. These experiments were done with the collaboration of workers at Chicago University who possess the necessary equipment.

3.0 LIST OF COMPOSITIONS

L-4-1	$\text{Li}_{.50}\text{Al}_{.35}\text{Fe}_{2.10}\text{O}_4$
L-4-4	$\text{Li}_{.50}\text{Al}_{.35}\text{Fe}_{2.14}\text{Co}_{.03}\text{O}_4$
L-4-6	$\text{Li}_{.50}\text{Al}_{.35}\text{Fe}_{2.14}\text{Co}_{.01}\text{O}_4$
L-4-7	$\text{Li}_{.50}\text{Al}_{.35}\text{Fe}_{2.14}\text{Co}_{.005}\text{O}_4$
L-7-0	$\text{Li}_{.50}\text{Al}_{.55}\text{Fe}_{1.92}\text{O}_4$
L-7-3	$\text{Li}_{.498}\text{Al}_{.55}\text{Fe}_{1.918}\text{Co}_{.005}\text{O}_4$
L-7-4	$\text{Li}_{.496}\text{Al}_{.55}\text{Fe}_{1.916}\text{Co}_{.0075}\text{O}_4$
L-7-5	$\text{Li}_{.495}\text{Al}_{.55}\text{Fe}_{1.915}\text{Co}_{.01}\text{O}_4$
L-7-6	$\text{Li}_{.499}\text{Al}_{.55}\text{Fe}_{1.919}\text{Co}_{.0025}\text{O}_4$
L-7-9	$\text{Li}_{.494}\text{Al}_{.55}\text{Fe}_{1.914}\text{Co}_{.0125}\text{O}_4$
L-7-10	$\text{Li}_{.497}\text{Al}_{.55}\text{Fe}_{1.917}\text{Co}_{.006}\text{Mn}_{.02}\text{O}_4$
L-8-1	$\text{Li}_{.498}\text{Al}_{.60}\text{Fe}_{1.868}\text{Co}_{.005}\text{O}_4$
L-8-2	$\text{Li}_{.496}\text{Al}_{.60}\text{Fe}_{1.866}\text{Co}_{.0075}\text{O}_4$
L-8-3	$\text{Li}_{.495}\text{Al}_{.60}\text{Fe}_{1.865}\text{Co}_{.01}\text{O}_4$
L-8-4	$\text{Li}_{.494}\text{Al}_{.60}\text{Fe}_{1.864}\text{Co}_{.0125}\text{O}_4$
L-8-5	$\text{Li}_{.497}\text{Al}_{.60}\text{Fe}_{1.867}\text{Co}_{.006}\text{Mn}_{.02}\text{O}_4$
L-9-0	$\text{Li}_{.495}\text{Al}_{.7}\text{Fe}_{1.74}\text{Co}_{.01}\text{O}_4$

L-9-1	$\text{Li}_{.494}\text{Al}_{.70}\text{Fe}_{1.74}\text{Co}_{.012}\text{O}_4$	
L-9-2	$\text{Li}_{.493}\text{Al}_{.70}\text{Fe}_{1.73}\text{Co}_{.014}\text{O}_4$	
L-10-0	$\text{Li}_{.499}\text{Al}_{.60}\text{Fe}_{1.799}\text{Co}_{.003}\text{Mn}_{.07}\text{O}_4$	
L-10-1	$\text{Li}_{.498}\text{Al}_{.60}\text{Fe}_{1.798}\text{Co}_{.005}\text{Mn}_{.07}\text{O}_4$	
L-10-2	$\text{Li}_{.496}\text{Al}_{.60}\text{Fe}_{1.796}\text{Co}_{.0075}\text{Mn}_{.07}\text{O}_4$	
L-10-3	$\text{Li}_{.497}\text{Al}_{.60}\text{Fe}_{1.797}\text{Co}_{.006}\text{Mn}_{.07}\text{O}_4$	
L-10-5	$\text{Li}_{.495}\text{Al}_{.60}\text{Fe}_{1.795}\text{Co}_{.010}\text{Mn}_{.07}\text{O}_4$	
L-11-0	$\text{Li}_{.495}\text{Al}_{.60}\text{Fe}_{1.78}\text{Co}_{.010}\text{Mn}_{.07}\text{O}_4$	
L-12-0	$\text{Li}_{.497}\text{Al}_{.60}\text{Fe}_{1.83}\text{Co}_{.006}\text{Mn}_{.02}\text{O}_4$	
L-12-1	"	
L-12-2	"	+ 1/4 wt.% ThO ₂
L-12-3	"	+ 1/2 wt.% ThO ₂
L-14-0	$\text{Li}_{.495}\text{Al}_{.60}\text{Fe}_{1.78}\text{Co}_{.010}\text{Mn}_{.07}\text{O}_4$	
L-14-1	"	
L-15-0	$\text{Li}_{.497}\text{Al}_{.60}\text{Fe}_{1.83}\text{Co}_{.006}\text{Mn}_{.02}\text{O}_4$	
L-16-1B	$\text{Li}_{.495}\text{Al}_{.60}\text{Fe}_{1.83}\text{Co}_{.010}\text{Mn}_{.02}\text{O}_4$	
L-16-2	$\text{Li}_{.492}\text{Al}_{.60}\text{Fe}_{1.83}\text{Co}_{.012}\text{Mn}_{.02}\text{O}_4$	
L-16-3	$\text{Li}_{.495}\text{Al}_{.60}\text{Fe}_{1.83}\text{Co}_{.010}\text{Mn}_{.02}\text{O}_4$	
L-16-6	$\text{Li}_{.493}\text{Al}_{.60}\text{Fe}_{1.83}\text{Co}_{.014}\text{Mn}_{.02}\text{O}_4$	
L-16-7	$\text{Li}_{.492}\text{Al}_{.60}\text{Fe}_{1.83}\text{Co}_{.016}\text{Mn}_{.02}\text{O}_4$	
L-12-B	$\text{Li}_{.497}\text{Al}_{.60}\text{Fe}_{1.83}\text{Co}_{.006}\text{Mn}_{.02}\text{O}_4$	
L-21-2	$\text{Li}_{.7}\text{Fe}_{1.9}\text{Ti}_{.4}\text{O}_4$	
L-21-3	$\text{Li}_{.85}\text{Fe}_{1.45}\text{Ti}_{.7}\text{O}_4$	

L-21-5	$\text{Li}_{.8}\text{Fe}_{1.4}\text{Cu}_{.1}\text{Ti}_{.7}\text{O}_4$
L-21-6	$\text{Li}_{.8}\text{Fe}_{1.2}\text{Cu}_{.1}\text{Mn}_{.2}\text{Ti}_{.7}\text{O}_4$
L-21-8	$\text{Li}_{.9}\text{Fe}_{1.3}\text{Ti}_{.8}\text{O}_4$
L-21-9	$\text{Li}_{.95}\text{Fe}_{1.15}\text{Ti}_{.9}\text{O}_4$
L-21-26	$\text{Li}_{.75}\text{Fe}_{1.35}\text{Cu}_{.2}\text{Ti}_{.7}\text{O}_4$
L-21-29	$\text{Li}_{.8}\text{Fe}_{1.3}\text{Mn}_{.1}\text{Cu}_{.1}\text{Ti}_{.7}\text{O}_4$
L-21-30	$\text{Li}_{.8}\text{Fe}_{1.6}\text{Ti}_{.6}\text{O}_4$
L-21-31	$\text{Li}_{.75}\text{Fe}_{1.55}\text{Ti}_{.6}\text{Cu}_{.1}\text{O}_4$
L-21-32	$\text{Li}_{.7}\text{Fe}_{1.5}\text{Ti}_{.6}\text{Cu}_{.2}\text{O}_4$
L-21-33	$\text{Li}_{.6}\text{Fe}_{1.4}\text{Ti}_{.6}\text{Cu}_{.4}\text{O}_4$
L-21-34	$\text{Li}_{.75}\text{Fe}_{1.54}\text{Ti}_{.6}\text{Cu}_{.1}\text{Mn}_{.01}\text{O}_4$
L-21-35	$\text{Li}_{.775}\text{Fe}_{1.425}\text{Ti}_{.65}\text{Cu}_{.1}\text{Mn}_{.05}\text{O}_4$
L-21-67	$\text{Li}_{.725}\text{Fe}_{1.525}\text{Ti}_{.55}\text{Cu}_{.1}\text{Mn}_{.1}\text{O}_4$
L-21-68	$\text{Li}_{.75}\text{Fe}_{1.3}\text{Ti}_{.7}\text{Cu}_{.2}\text{Mn}_{.05}\text{O}_4$

4.0 LITHIUM-ALUMINUM COMPOSITIONS

The $4\pi M_s$ range which is given as a requirement in Section 1.0 represents a significant reduction relative to the $4\pi M_s$ of $\text{Li}_{0.5}\text{Fe}_{2.5}\text{O}_4$. A reduction in magnetization is usually accomplished by the replacement of octahedral Fe^{3+} by diamagnetic ions. Aluminum ions have been employed for this purpose in lithium ferrites [Ref. 3 and in other ferrites [Ref. 4]. Thus, a number of compositions in the lithium-aluminum ferrite system were explored.

4.1 Materials with $4\pi M_s \approx 1800$ Gauss

In Table I, measurements of coercive force (H_c), saturation magnetization ($4\pi M_s$), remanence (B_r), $B_r/4\pi M_s$, resistivity, and density are given for a number of compositions and firing conditions. In Table II, linewidth data are presented, and a graphic representation of some of the linewidth data is displayed in Fig. 4. Figure 5 shows the dependence of resistivity on two of the important experimental parameters, cobalt content and firing temperature. Finally, density as a function of firing temperature is shown in Fig. 6.

4.1.1 Effect of Cobalt Addition on Linewidth

In an investigation involving linewidths of polycrystalline materials, several factors must be considered. There are factors which are intrinsic to "single crystal linewidth," and those which are related to polycrystallinity. In the case of stoichiometric lithium-aluminum ferrites, the former should not be important. "Fast-relaxing" impurities are not present, and it has been shown that lithium ferrite single crystals

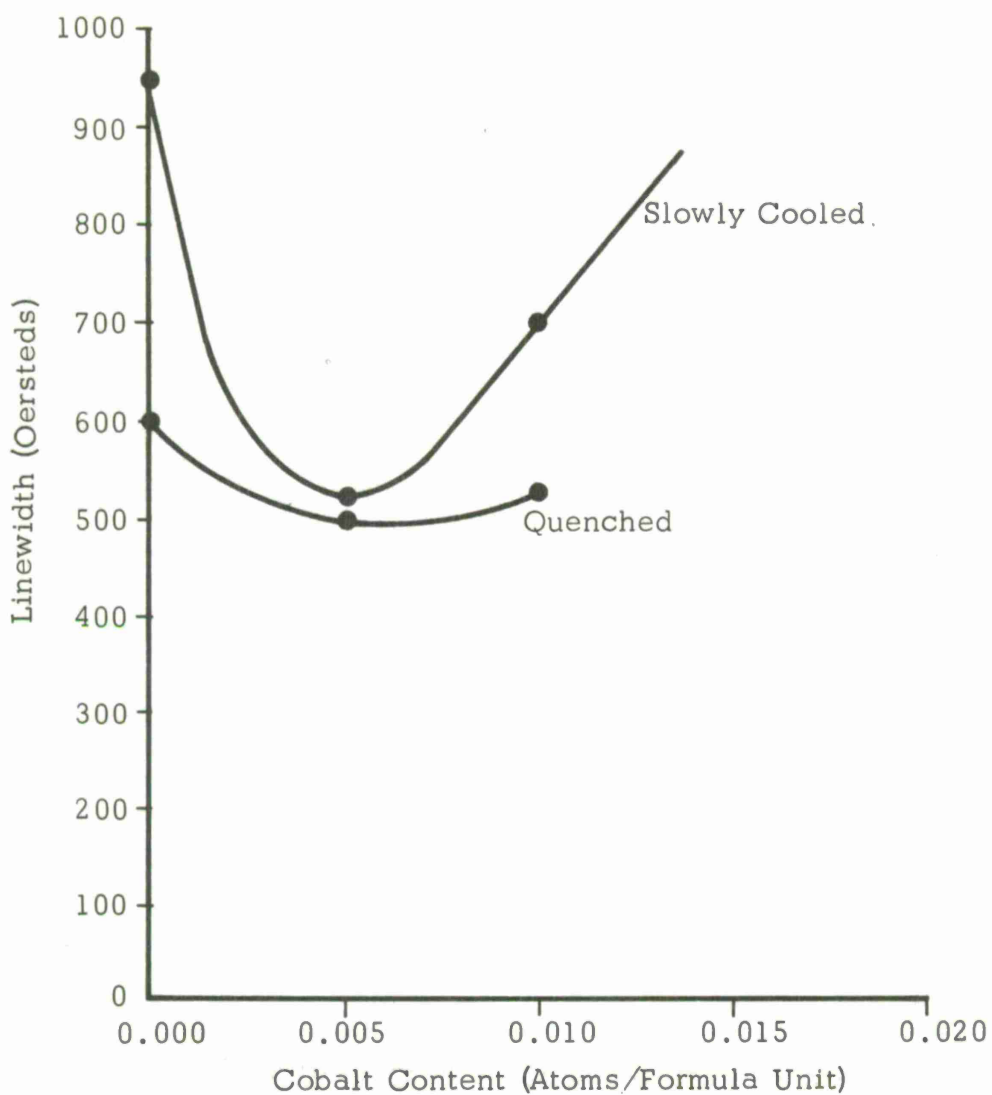


Fig. 4 Resonance Linewidth vs. Cobalt Content in the L-4 Series (Firing Temp. = 1175° C)

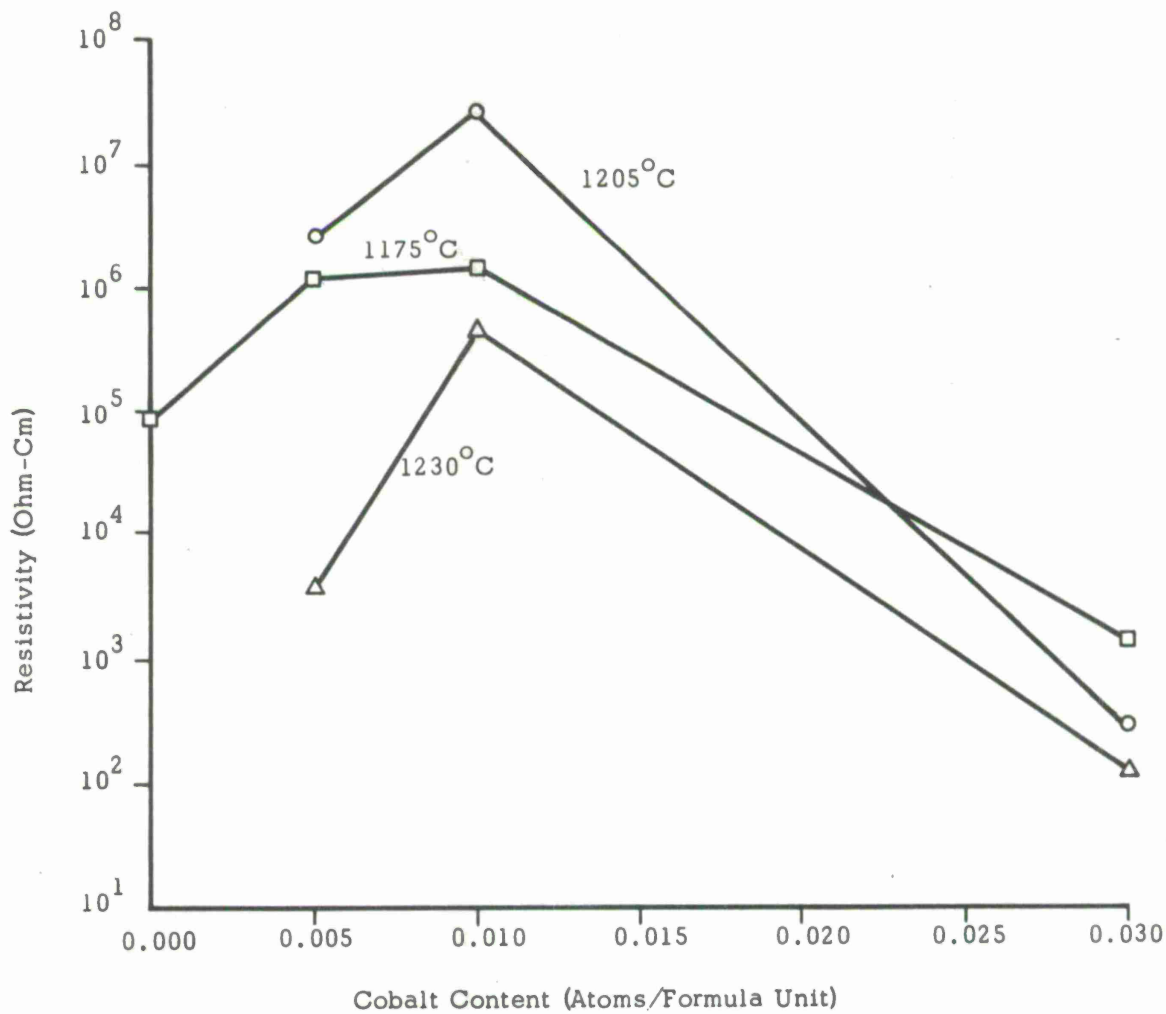


Fig. 5 Resistivity vs Cobalt Content in the L-4 Series

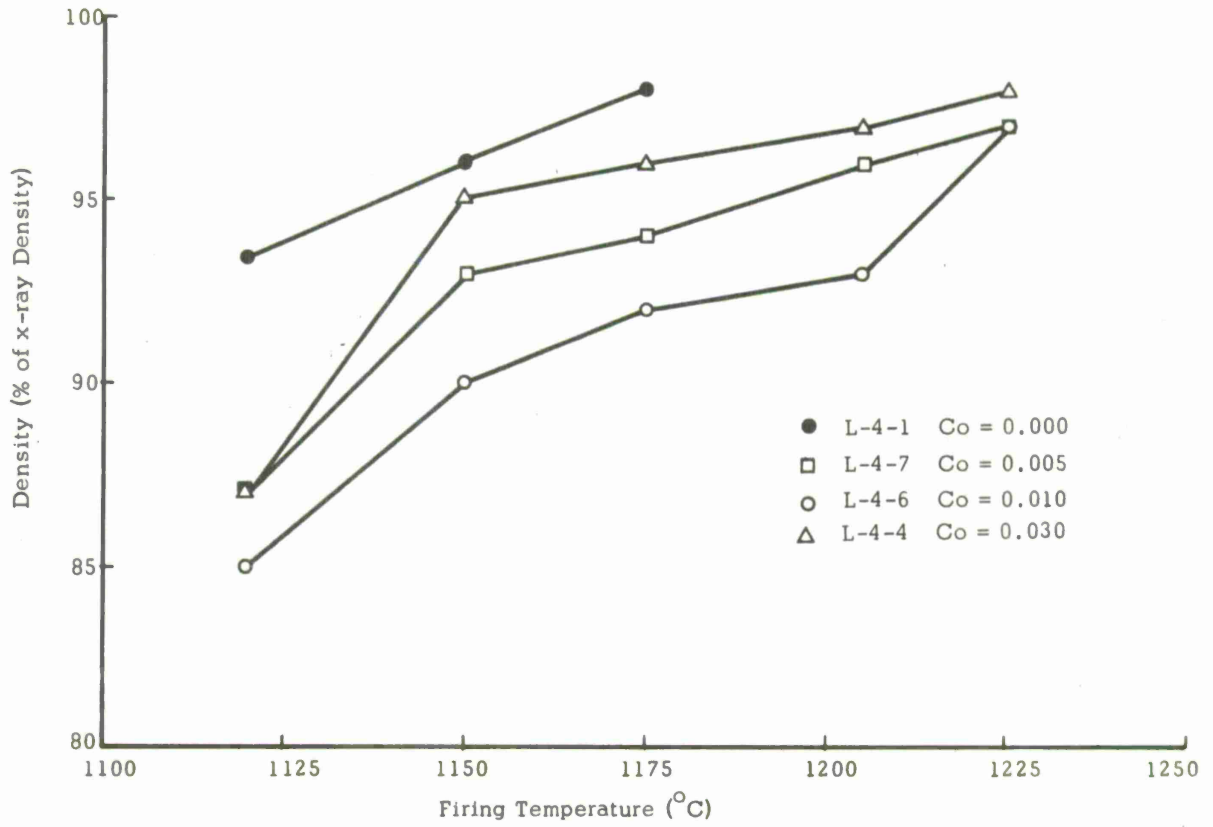


Fig. 6 Density vs. Firing Temperature in the L-4 Series

Table I. Representative Data for Lithium Aluminum Ferrites
of $4\pi M \approx 1800$ G.

SAMPLE	Firing Temp. (°C)	Firing Atm.	H _c (Oe)	4πM _s (gauss)	B _r (gauss)	$\frac{B_r}{4\pi M_s}$	Resistivity After Grinding (ohm-cm)	Density (% x-ray density)
L-4-1	1150	O ₂	10.0	1800	1210	0.67	4.3×10 ⁵	96
	1175	O ₂	8.8	1810	1210	0.67	9.7×10 ⁴	98
L-4-4	1150	O ₂	17.5	1650	575	0.35	1.6×10 ⁵	95
	1175	O ₂	16.0	1620	445	0.27	1.8×10 ³	96
	1205	O ₂	15.0	1635	445	0.27	5.6×10 ²	97
	1230	O ₂		1620	440	0.27	1.8×10 ²	98
L-4-6	1150	O ₂	11.0	1820	575		1.3×10 ⁵	90
	1175	O ₂	9.5	1790	570		2.5×10 ⁶	92
	1205	O ₂	8.2	1810	380		4.7×10 ⁷	93
	1230	O ₂	6.8	1830	955		6.5×10 ⁵	97
L-4-7	1150	O ₂	8.8	1755	1120	0.64	2.2×10 ⁶	93
	1175	O ₂	8.8	1800	1150	0.64	1.4×10 ⁶	94
	1205	O ₂	8.2	1810	1210	0.67	4.0×10 ⁶	96
	1230	O ₂	6.8	1850	890	0.48	5.5×10 ³	97

have extremely narrow linewidths [Ref. 5]. The polycrystalline factors have been shown by Schlomann [Ref. 6] to depend on an anisotropy term, $|K_1/M_s|$, and a term which is proportional to the product of the porosity and the magnetization. The porosity term is only about 150 Oe in a 2000-gauss ferrite of 5% porosity and is less at lower magnetizations and porosities.

Sirvetz and Saunders [Ref. 7] were able to compensate the negative K_1 of nickel ferrite by the addition of cobalt, which makes a positive contribution to K_1 . Their result was a minimum linewidth where the compensation was an optimum. Although divalent cobalt, a "fast-relaxing" impurity, can add to the "single crystal linewidth," its potential for reducing K_1 was considered attractive.

Table II. Resonance Linewidth and Density Data for Lithium Aluminum Ferrites of $4\pi M_s \approx 1800$ G

Sample	Sintering Temp. ($^{\circ}$ C) In Oxygen	$4\pi M$ (gauss)	Density (% of x-ray density)	Linewidth (Oe) After Slow Cooling	Linewidth (Oe) Quenched From 870° C
L-4-1	1150	1800	96	1100	800
	1175	1810	98	950	600
L-4-6	1175	1790	92	700	550
	1205	1810	93	380	
L-4-7	1175	1800	94	520	500
	1205	1810	96	450	

The effect of cobalt addition is summarized in Table II and depicted graphically in Fig. 4. The optimum compensation of K_1 and the minimum linewidth occurs at a cobalt content of 0.005 atoms per formula unit. This same procedure could, in principle, be applied to the lower saturation magnetization materials.

4. 1. 2 Effect of Order-Disorder on Linewidth

As may be seen in Fig. 4, and also by comparing the data in the last two columns of Table II, lower linewidths are produced by quenching from 870° C than by slow cooling.

Although lower linewidths are obtained in quenched samples, as opposed to slowly cooled samples, a severe cracking problem in the large samples needed for device applications prohibits the use of quenching. However, as demonstrated in Fig. 4, the minimum values of linewidths are comparable for both quenched and slowly cooled samples.

4. 1. 3 B-H Loop Properties

The primary B-H loop properties of interest in this program are H_c and the ratio of B_r to $4\pi M_s$. As seen in Table I, the effect of cobalt on the coercive force is somewhat comparable to the effect on linewidth. Since the coercive force depends on $|K_1/M_s|$ as does the linewidth, the similarity of behavior may be expected. The effect is masked somewhat by variations in microstructure as evidenced by comparison of density values. Microstructural parameters such as grain size, grain shape, and nonmagnetic inclusions distinctly influence the coercive force. The coercive force values in Table I generally are considerably higher than desired, which at least in part indicates the difficulty of obtaining well-sintered lithium-aluminum ferrites.

The ratio $B_r/4\pi M_s$ is also affected by the addition of cobalt. For small additions, there is not a large decrease in this parameter when compared to the L-4-1 composition containing no cobalt. With larger amounts of cobalt present, $B_r/4\pi M_s$ is distinctly lower. This is the expected behavior from the theory of Wijn et. al [Ref. 8], since the sign of K_1 changes from negative to positive with the increase in cobalt content.

4. 1. 4 Resistivity

In Fig. 5 resistivity is plotted as a function of cobalt content. The reasons for the maxima in the curves are not completely understood.

4. 1. 5 Density

The density of several compositions is shown as a function of firing temperature (Fig. 6). As is seen, density increases with temperature in a manner typical of such ceramic systems. Although densities in excess of 95% were obtained, the grain sizes of the materials were generally small and not as uniform as desired.

4. 2 Materials with $4\pi M_s \simeq 800$ Gauss

Several series of compositions (L-7, L-8, and L-10) were formulated to investigate the 800 gauss region of $4\pi M_s$ values. The magnetizations and B-H data of these materials are presented in Table III. In addition, the measurements of the magnetizations of two garnets are included for reference.

The L-7 compositions contain 0.55 aluminum atom per formula unit and magnetizations of approximately 900 gauss. The L-8 and L-10 materials contain 0.60 aluminum atom per formula unit and have magnetizations of about 700 gauss. Within each series there are variations of cobalt and other minor element contents, and these are shown in Table III. The remanence (B_r) to saturation magnetization ($4\pi M_s$) ratios are sufficiently high for most of the samples, especially for those with moderate cobalt addition. Coercive force values (H_c) are again higher than desired.

4. 2. 1 Linewidth Data

In Table IV, linewidths, densities, and resistivities are given for a number of L-7 compositions with the firing treatment as a parameter. The furnace atmosphere was oxygen in all cases. In addition, the linewidth as a function of cobalt content is presented in Fig. 7 for several sintering temperatures. The sintering time was held constant at three hours for all the data in Fig. 7. The curve in Fig. 7 shows that cobalt is effective in lowering linewidths.

Because the linewidth partially depends on the anisotropy, and because the anisotropy is negative for most ferrites, cobalt's positive contribution to anisotropy usually lowers the linewidth. When the optimum amount of cobalt is surpassed, the anisotropy field becomes positive and increases. Therefore, the linewidth increases. A minimum in the curve is expected, and is demonstrated in Fig. 7.

Table III. Properties of Lithium Aluminum Ferrites
of $4 \pi M_s \approx 800$ Gauss

Sample	Co ²⁺ atoms per formula unit)	$4 \pi M_s$ (Gauss)	B _R (Gauss)	$\frac{B_R}{4 \pi M_s}$	H _C (Oersteds)
L-7-0	0.000	903	645	0.71	9.2
L-7-3	0.005	862	557	0.65	9.7
L-7-5	0.010	865	485	0.56	9.5
L-7-6	0.0025	848	575	0.68	9.4
L-7-9	0.0125	885	510	0.58	10.0
L-7-10	0.006	870	633	0.73	8.5
L-8-1	0.005	676	443	0.66	12.0
L-8-3	0.010	670	284	0.42	14.6
L-8-4	0.0125	687	326	0.47	12.6
L-8-5	0.006	700	412	0.59	13.0
L-10-1	0.005	730	484	0.66	13.0
L-10-2	0.0075	737	487	0.66	14.3
L-10-3	0.006	713	490	0.69	15.0
L-10-4	0.006	720	284	0.40	14.3
L-10-5	0.010	717	527	0.73	14.0
Aluminum Garnet		427			
Gadolinium Garnet		763			

Examination of several of the properties of interest as a function of sintering temperature is informative in demonstrating the difficulty of optimizing all parameters. Figure 8 shows the linewidth behavior versus sintering temperature for a number of representative compositions. Figure 9 displays ranges of densities versus sintering temperature of the L-8, L-9, and L-10 compositions.

Table IV. Properties of Lithium Aluminum Ferrites of L-7 Series

Sample	Firing Temp. (°C)	Firing Time (Hours)	Density (% x-ray density)	Linewidth (oersteds)	Resistivity (ohm-cm)
L-7-0	1150	3	93.0	650	$>10^9$
	1175	18.5	97.7	800	2.0×10^6
	1205	3	96.8	800	2.7×10^5
L-7-6	1150	3	92.5	640	
	1175	3	97.3	450	6.3×10^4
	1175	18.5	98.2	620	6.2×10^5
	1205	3	96.6	550	8.8×10^4
L-7-3	1150	3		400	
	1150	43	97.5	280	8.2×10^5
	1175	3	97.0	225	1.4×10^5
	1175	18.5	97.3	370	1.2×10^6
	1205	3	96.6	330	9.1×10^4
L-7-4	1175	3	97.5	230	1.4×10^5
	1175	18.5	97.7	240	1.8×10^6
	1205	3	97.3	270	2.7×10^5
L-7-5	1150	3	93.0	570	6×10^7
	1205	3		760	
L-7-9	1205	3		1400	

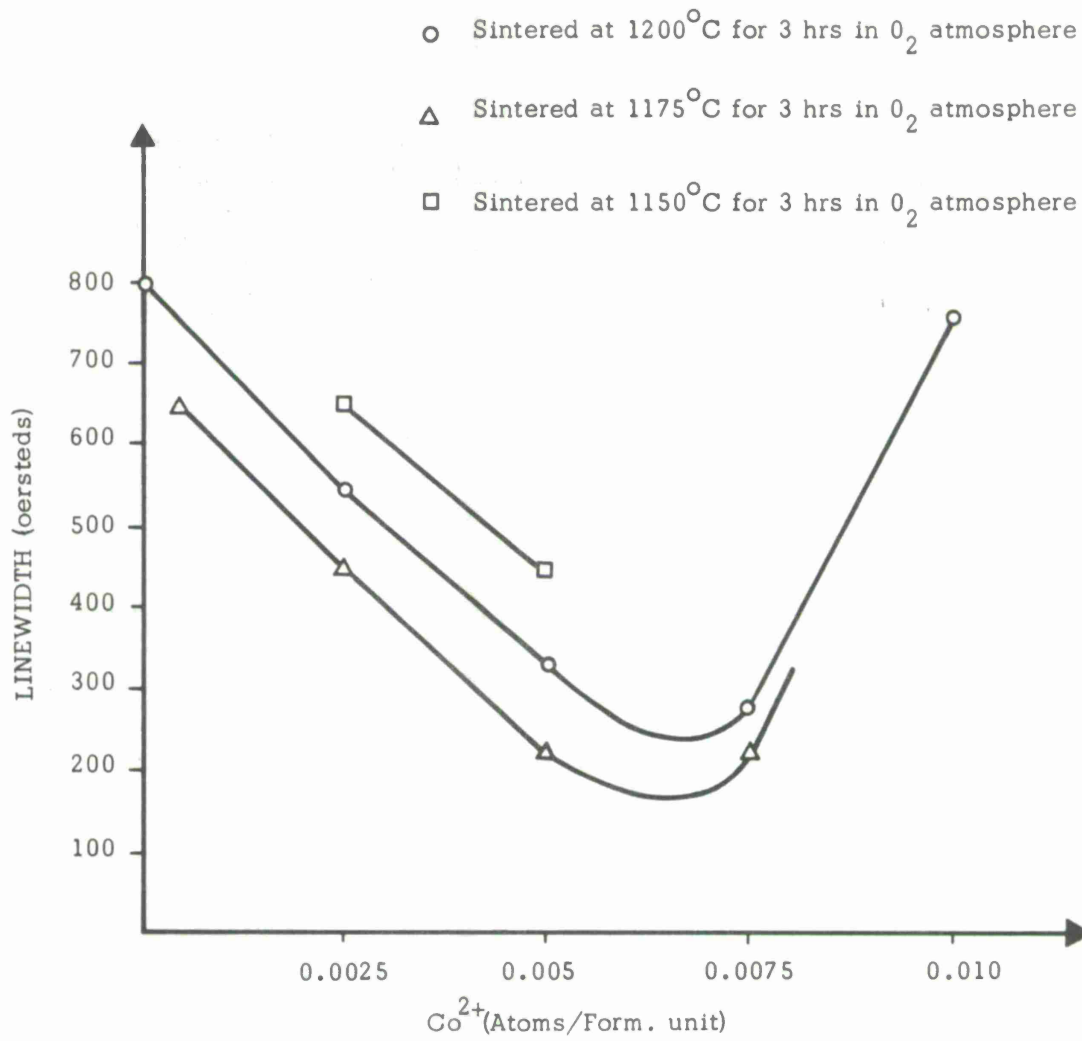


Fig. 7 Linewidth Versus Cobalt Content for the L-7 Series of Compositions

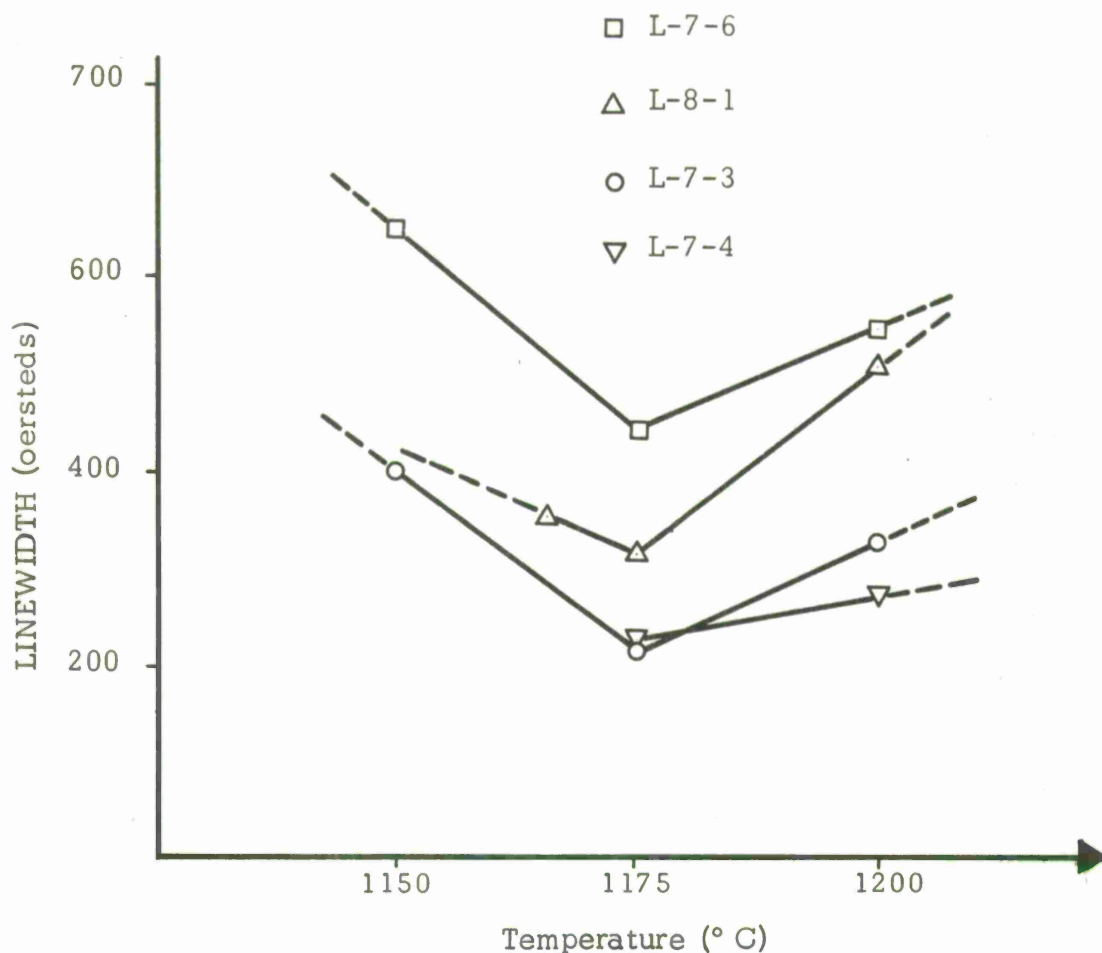


Fig. 8 Linewidth Versus Sintering Temperature for a Number of Representative Samples

4.3 Magnetic and Dielectric Loss

During the course of the investigation, it was found that low-field magnetic losses were very high in most of the lithium ferrites which had been submitted to Lincoln Laboratory for evaluation. Several high-loss samples were examined microscopically and all showed discontinuous grain growth (extreme variations in grain size). One of the worst cases, a micrograph of composition L-8-5, is shown in Fig. 10a. In Fig. 10b, the microstructure of a garnet is shown for comparison. At this point, efforts

were made to determine the causes of the low-field magnetic losses. Microstructural factors were considered important in this respect and therefore were given considerable attention.

Two compositions were selected, L-8-5 and L-10-5; in which the major substitution was 0.6 atoms of Al^{3+} per formula unit. The criteria for selection were low linewidths and high resistivities which had been determined in past experiments.

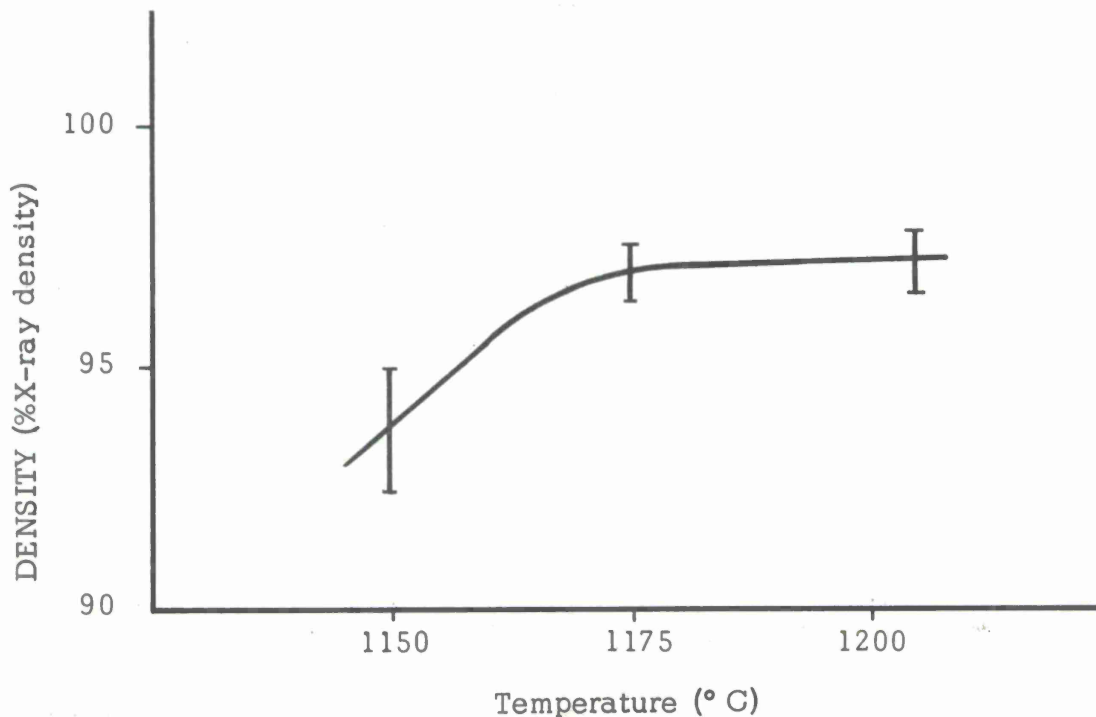


Fig. 9 Density Ranges Versus Sintering Temperature for the L-7, L-8, and L-10 Series of Samples

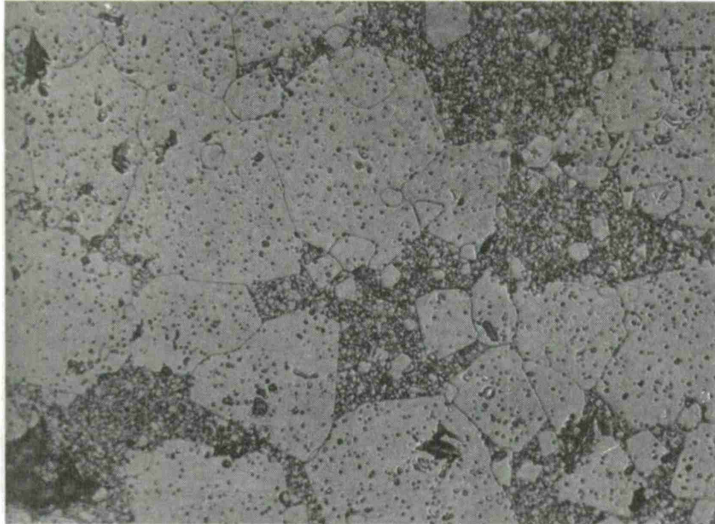


Fig. 10a

L-8-5

1175° C - 3 Hrs.

1 cm = 32 μ

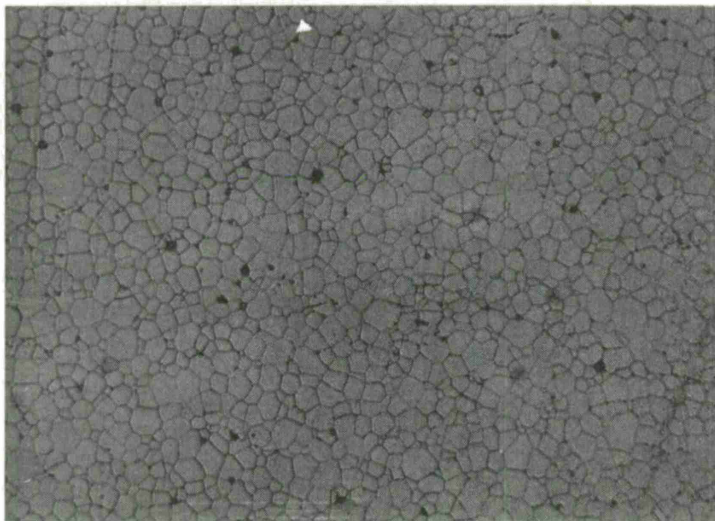


Fig. 10b

Garnet

1 cm = 33 μ

4.3.1 Experimental Details

Compositions L-12-0, L-12-1, L-12-2, L-12-3, and L-16-1B all had the same formula as composition L-8-5. L-12-0 was prepared by standard processing, which included the use of polyvinyl alcohol (PVA) as the binder. This composition was fabricated to determine if the elimination of intermixing in the ball-milling step would eliminate discontinuous grain growth. In L-12-1, L-12-2, and L-12-3 an acrylic binder was substituted for PVA. Furthermore, thorium oxide was added as a grain growth inhibitor [Ref. 9] to L-12-2 and L-12-3 in the quantities, 1/4 weight-percent and 1/2 weight-percent, respectively. L-16-1B employed $\text{Al}(\text{OH})_3$ as the source of aluminum. It was felt that this raw material might be more reactive than Al_2O_3 and might yield a more homogeneous product.

Compositions L-11-0, L-14-0, and L-14-1 had the formula of composition L-10-5. L-11-0 was prepared by standard processing similarly to L-12-0. L-14-0 and L-14-1 both employed $\text{Al}(\text{OH})_3$ as the source of aluminum ions, with L-14-0 containing a wax binder and L-14-1 containing an acrylic binder.

Composition L-9-0 contained a greater quantity of aluminum than the other compositions so that the effect of lowering $4\pi M_s$ could be evaluated. L-9-0 had 0.7 atoms of Al^{3+} and 0.01 atoms of Co^{2+} . The cobalt was included to lower the anisotropy field. The processing of this material was like that of L-11-0 and L-12-0 in that Al_2O_3 was the source of aluminum ions and PVA was the binder.

4.3.2 Results of Loss Studies

The results of density, low-field magnetic loss, and dielectric loss measurements are presented in Table V for the various compositional and processing variations. Variations from the standard methods of processing are included in the column headed "Processing Variables." The

Table V. Loss Data and Density Values as a Function of Composition, Processing Variables, and Firing Treatment

SAMPLE NO.	FIRING TEMP/TIME ° C/h	PROCESSING VARIABLES	DENSITY (% X-RAY)	MAGNETIC LOSS (DB)	DIELECTRIC & DEVICE LOSS (DB)
L-4-1	1150/3		95	9.3	2.96
L-4-4	1150/3		95	4.8	1.66
L-7-0	1150/40			>10	1.36
	1175/18		98	>10	2.74
L-7-4	1150/40			3.9	1.38
	1175/18		98	6.0	2.54
L-8-1	1150/3		95	1.35	0.52
	1175/3		97	6.10	1.48
L-8-4	1150/3		95	0.86	0.52
	1175/3		98	1.95	1.40
L-10-3	1175/3		97	>10	0.36
L-10-5	1175/3		97	8.5	0.36
L-11-0	1150/5		95	>10	0.45
	1205/5		97.5	9.7	0.44
L-12-0	1150/5		95	3.5	0.47
	1175/5		96	5.6	0.40
	1205/5		97	6.1	0.44
	1205/5		97	>10	0.53
L-12-1	1150/5	Acrylic binder	95	8.3	0.54
	1175/5	Acrylic binder	96.5	>10	0.65
	1205/5	Acrylic binder	97.5	>10	
L-12-2	1150/5	Acrylic binder	93.5	1.9	0.67
	1175/5	Acrylic binder	96	5.3	0.46
	1205/5	Acrylic binder	97	>10	
L-12-3	1150/5	Acrylic binder	91.5	1.2	0.54
	1175/5	Acrylic binder	94	2.45	0.40
	1205/5	Acrylic binder	96.5	>10	
L-14-0	1175/5	Al(OH) ₃ ; wax binder	87	1.03	0.46
	1175/5	Al(OH) ₃ ; wax binder	85	0.84	1.90
	1205/5	Al(OH) ₃ ; wax binder	90	1.73	0.50
L-14-1	1150/5	Al(OH) ₃ ; Acrylic binder	89	1.9	0.67
	1175/5	Al(OH) ₃ ; Acrylic binder	93.5	>10	0.41
L-15-0	1150/5	Al(OH) ₃	89	2.3	0.60
	1175/5	Al(OH) ₃	93.5	6.5	0.46
	1205/5	Al(OH) ₃	95	>10	1.22
		Gadolinium Garnet		0.50	0.40

binder employed in the standard method is polyvinyl alcohol (PVA). Unless another binder is stipulated in Table V, it is to be assumed that PVA was used. Aluminum oxide was normally used as a source of aluminum except where Al(OH)_3 is indicated.

The processing variable which appears to yield the most consistent behavior is the firing temperature. In examining the data in Table V, it may be seen that in almost all cases the loss increases with firing temperature. Unfortunately, at least two variables are changing simultaneously with firing temperature, so that it is difficult to determine definitely which is responsible for the loss. Both grain size and density increase with the firing temperature. In addition, certain chemical changes, such as reduction and lithium volatilization, are also possible and may be important as higher firing temperatures are employed. One factor, observed in most of the compositions, and which is indicative of a possible chemical change, is a linewidth which is higher for a 1205°C firing than for a 1175°C firing. Because the density is greater for the 1205°C firing than for the 1175°C firing, a lower linewidth would be expected for the higher temperature if the chemistry were identical.

One experiment which was designed to give some insight into the effect of grain size was the addition of thorium oxide to a few compositions to inhibit grain growth [Ref. 9]. The L-12-1, L-12-2, and L-12-3 compositions were all prepared identically, except that 1/4 weight-percent ThO_2 was added to L-12-2 and 1/2 weight-percent ThO_2 was added to L-12-3. Each of these compositions was fired at 1150°C , 1175°C , and 1205°C for five hours. The micrographs for the 1175°C firing are shown in Figs. 11 through 13. The grain growth inhibiting action of the thoria is clearly demonstrated. The thoria-doped materials are also seen to have more uniform microstructures and lower losses than the control material.

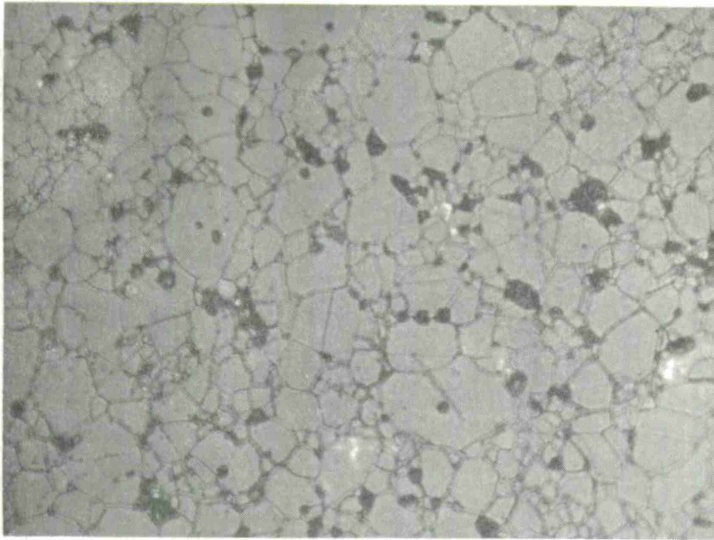


Fig. 11
L-12-1
1175° C - 5 Hrs.
1 cm = 11 μ

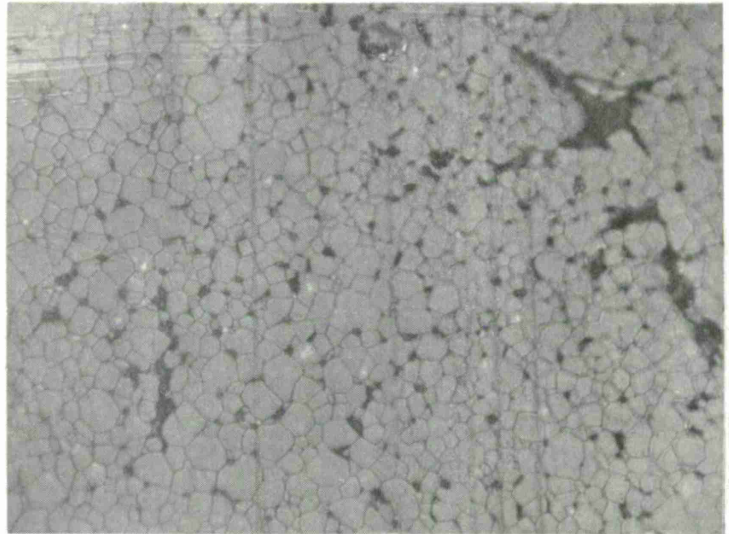


Fig. 12
L-12-2
1175° C - 5 Hrs.
1 cm = 11 μ

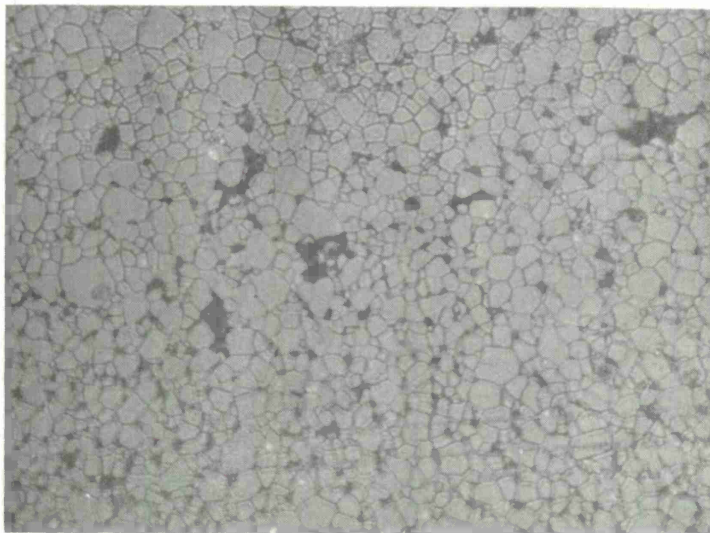


Fig. 13
L-12-3
1175° C - 5 Hrs.
1 cm = 11 μ

The use of the $\text{Al}(\text{OH})_3$ appears to result in a lower density than when using Al_2O_3 . This may be seen by comparing the densities in Table V for L-15-0 to L-12-0. These compositions should be identical except for the different source of aluminum ions. The other compositions which were processed using $\text{Al}(\text{OH})_3$ are L-14-0 and L-14-1. Both of these have relatively low densities. Because the calcining and milling treatments were not optimized, the best sintering conditions for the $\text{Al}(\text{OH})_3$ materials were probably not achieved.

The various binders used on the program yielded a variety of microstructures for given firing treatment, which demonstrates the importance of the processing procedures in determining the microstructure and the low-field magnetic loss. The compositions L-12-0 and L-12-1 are identical except for the binders employed. By comparing the data in Table V for these compositions and by examining Figs. 14 and 15, large variations in data and microstructures can be seen.

Linewidth, magnetization, and B-H loop data are presented in Tables VI and VII for a number of the compositions whose loss properties were included in Table V.

Several compositions which had been prepared during earlier phases of the program were also evaluated in the phase-shifter. These were the compositions L-4-1, L-4-4, L-7-0, L-7-4, L-8-1, L-8-4, L-10-3, and L-10-5. The data on these materials are also listed in Table VI.

Two series of compositions which differed in saturation magnetization were fabricated to determine the effect of the magnetization on the magnetic loss. The L-9 compositions had 0.70 aluminum atoms-per-formula-unit substituted for iron, whereas in the L-16 compositions, 0.60 aluminum atoms-per-formula-unit were substituted. Within the L-9 series, the only variable was the cobalt content. Other factors, such as

Table VI. Linewidth as a Function of Composition and Firing Treatment

SAMPLE NO.	FIRING TEMP/TIME (° C/HR)	LINEWIDTH (OERSTEDS)
L-11-0	1150/5	750
	1175/5	900
L-12-0	1175/5	800
L-12-1	1150/5	720
	1175/5	800
L-12-2	1150/5	720
	1175/5	760
L-12-3	1150/5	630
	1175/5	720
L-14-0	1175/5	650
L-14-1	1175/5	780
L-15-0	1175/5	820
L-16-1B	1175/5	400

the source of aluminum ions and type of binder, were kept constant. In the L-16 series, the cobalt content was again a variable. Furthermore, several types of binders were employed. L-16-1 contained polyvinyl alcohol as the binder. A wax binder was used in L-16-1B and an acrylic binder in L-16-3.

The results of the various measurements on the L-9 and L-16 series of compositions are presented in Table VIII. The L-9 compositions

Table VII. Hysteresis Loop and Magnetization Data as a Function of Composition and Firing Treatment

SAMPLE NO.	FIRING TEMP/TIME (°C) (HRS.)	H _C (OERSTEDS)	B _r (GAUSS)	4πM _s (GAUSS)	B _r /4πM _s
L-11-0	1150/5	13.0	490		
	1175/5	11.5	490	920	0.53
L-12-0	1150/5	16.3	405		
	1175/5	11.0	443	637	0.70
L-12-1	1150/5	17.3	387		
	1175/5	12.2	420	648	0.65
L-12-2	1150/5	15.7	383		
	1175/5	16.0	320	712	0.45
L-12-3	1150/5	14.4	387		
	1175/5	16.0	343	585	0.59
L-14-0	1175/5	12.2	330	557	0.59
L-14-1	1150/5	13.6	378		
	1175/5	13.0	383	566	0.68
L-15	1150/5	14.6	354		
	1175/5	12.5	332	572	0.58

Table VIII. Compilation of the Data for the L-9 and L-16 Series of Compositions

Composition Number	Firing Temp./Time (°C/Hours)	Magnetic Loss (db)	Dielectric Loss (db)	ΔH @ 9.8 Gc (oe)	ΔH @ 2.8 Gc (oe)	Density (% x-ray)	Resistivity (Ohm-cm)	$4 \pi M_s$ (Gauss)	B_r (Gauss)	H_c (oe)
Gd Garnet		0.60	0.42	220				725		
L-9-0	1175/5	0.90	0.49	400		87	7.0×10^6	380	90	
	1175/9	0.90	0.50	410		91	2.6×10^7	368		8.5
	1175/9	0.91	0.50		279	92	2.0×10^7		114	
	1175/12								148	7.2
	1175/15	0.70	0.72	420		95	1.0×10^7	379		
L-9-1	1175/9	1.10	0.55		637	95	2.2×10^5			8.8
L-9-2	1175/9	1.80	1.76		710	97	1.6×10^5			7.2
L-16-1	1175/5	0.87	0.45	360	391	88	1.0×10^7	599	330	7.7
	1175/9	0.90	0.57	650		91	3.0×10^7	592		
	1175/15	1.70	0.45	570		94	1.0×10^8	637		
L-16-1B	1150/3	0.86	0.45							
	1175/3	0.85	0.45							
	1175/5	1.64	0.49	400	555	91	3.8×10^8	595	415	12.0
	1175/9	1.30	0.45	480		94	1.0×10^8	613		
	1175/15	8.00	1.04	650		96	1.3×10^7	708		
L-16-3	1175/9	5.00	0.50		755	95	3.5×10^6		450	10.4
L-16-2	1175/9	1.00	0.50		369	89	2.2×10^7		320	11.3
	1175/12								330	10.8
L-16-6	1175/5	1.20	0.54	320	247	92	2.6×10^8	640	318	8.4
	1175/9	2.12	0.64		299	94	4.5×10^7		378	8.5
L-16-7	1175/5	1.76	0.49	370	273	93	1.2×10^8	682	340	10.6

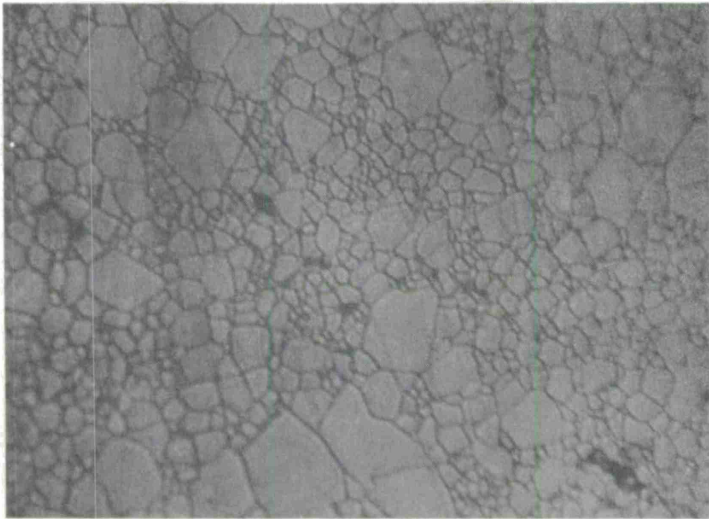


Fig. 14

L-12-0
1175° C - 5 Hrs.
1 cm = 11 μ

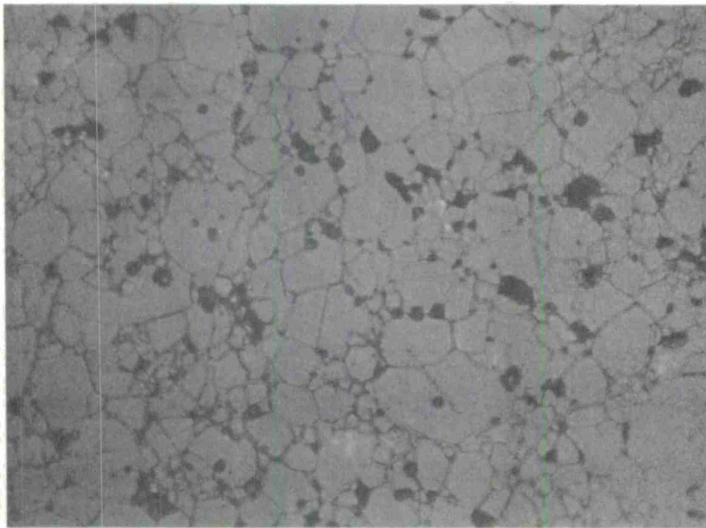


Fig. 15

L-12-1
1175° C - 5 Hrs.
1 cm = 11 μ

yielded relatively low magnetic losses. However, this result is not dramatic considering the low $4\pi M_s$ values of the L-9 series. Within both the L-9 and L-16 series, there appeared to be a small dependence of the magnetic loss on the cobalt content. However, the lack of uniform microstructures and high densities prevented a conclusion as to the effect of this parameter.

Examination of the results for a single composition prepared with several different binders (i. e. , L-16-1, L-16-1B, and L-16-3) shows distinct differences in the magnetic loss. These data again demonstrate the importance of the conditions prior to the firing treatment in determining the final properties of a given composition.

The firing time and temperature exert a very significant influence over not only the magnetic loss, but also density, dielectric loss, linewidth, magnetization, and coercive force. Generally, the data show that the magnetic losses and dielectric losses increase with firing temperature and time. There are few situations where minor deviations from the stated behavior arose.

Another interesting effect which is relatable to the the firing conditions is a change in the shape of the microwave resonance curve as the firing time is varied. An example of such a change in shape is shown Fig. 16. The sharp rise in magnetization and the change in the shape of the resonance curve are probably indicative of some chemical change occurring in the material, causing inhomogeneity. These effects may be attributable to processes such as lithium volatility, iron reduction, or slow diffusion of the aluminum ions from octahedral to tetrahedral sites. The time dependence indicated that equilibrium was not being attained in these experiments. As a result, inhomogeneities may be present which are detrimental to the losses, linewidth, coercive force, etc.

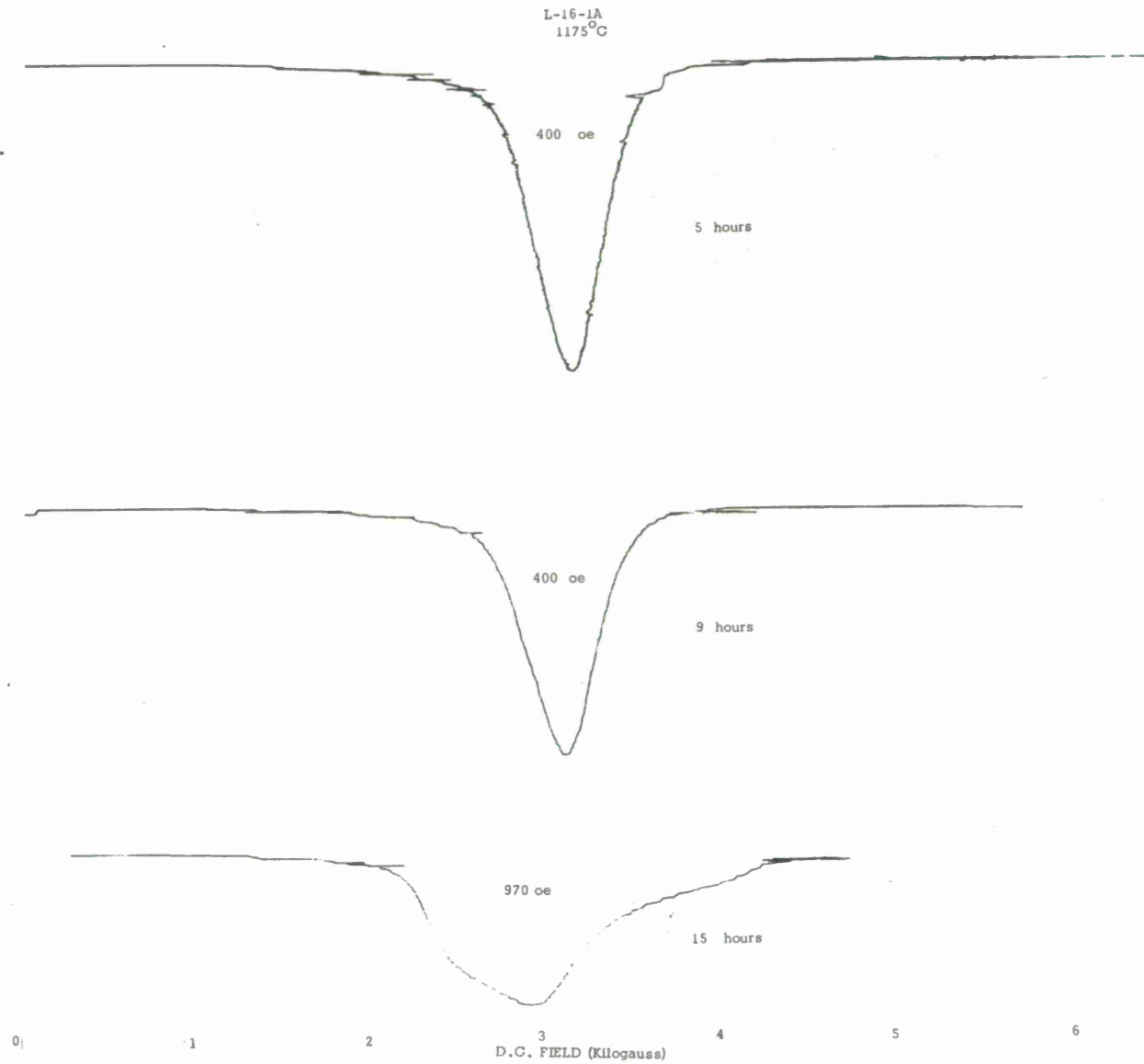


Fig. 16 Resonance Curve Shapes for Composition L-16-1A Fired at 1175° C for 5, 9, and 15 Hours.

4.3.3 Results of Isostatic Pressing on Microstructure

Because of the importance of the uniformity of microstructure to the magnetic properties, the utilization of isostatic pressing was explored. The technique of isostatic pressing has been employed extensively to obtain uniform and dense products in a variety of ceramic applications.

The composition L-12-B, with 0.6 atoms of Co^{2+} per formula unit, was selected for this experiment, because of microstructural evidence which was available for samples of this composition which contained binders and had been prepared by conventional dry-pressing.

Pieces of the pressed and unfired samples were formed into regular shapes and the "green" densities were measured. The samples were then fired at 1175°C for five hours in oxygen.

After the samples were fired, pieces were cut and formed into regular shapes for density measurements. Samples were also cut, polished, and thermally etched for microstructure examination.

Generally, it was found that isostatic pressing did not lead to significantly higher densities than obtained in the conventionally pressed materials, but the microstructures of the isostatically pressed materials were usually more uniform. A representative micrograph is shown in Fig. 17. The grain sizes of isostatically pressed materials were still smaller than desired.

4.4 Conclusion

Many difficulties were encountered in sintering lithium-aluminum ferrites. The combination of the refractory nature of aluminum oxide, requiring high firing temperatures, and lithium volatility, requiring

low firing temperatures, was a limitation which prevented the attainment of uniform microstructures, low coercive forces, and satisfactory microwave properties. Additional work on ceramic processing (i. e. , calcining milling, binders, etc.) might have proved beneficial in this respect. However, it was found that the lithium-titanium ferrite system sintered better and showed more promise for obtaining good magnetic properties.

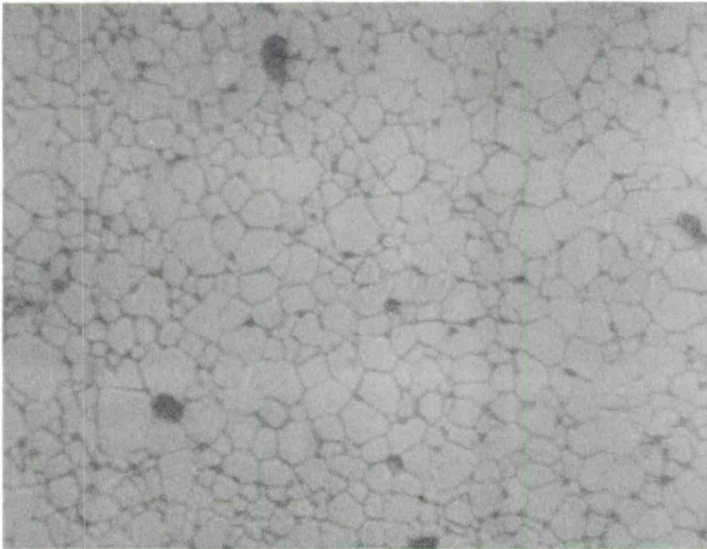


Fig. 17
L-12-B-9
1175° C - 5 Hrs.
1 cm = 11 μ

5.0 LITHIUM-TITANIUM FERRITES

5.1 General

Because of the problems associated with the substitution of aluminum for iron in the lithium ferrites, other possible substitutional ions were considered as parallel approaches to the lithium-aluminum ferrites. Lithium-titanium ferrites proved to offer advantages over the lithium-aluminum system. The properties of L-21-2 and L-21-3 (0.7 and 0.4 atoms/formula unit, respectively) are given in Table IX. The coercive forces are lower than found in the lithium-aluminum ferrites and the remanence ratios are greater than 0.7.

The Curie temperature decreases somewhat faster for the titanium additions than for aluminum additions. This behavior is probably caused by the greater content of lithium in the formula. The extra Li^{1+} ion is added to balance the Ti^{4+} which has replaced Fe^{3+} .

The microstructure of the L-21-2 sample is presented in Fig. 18. The microstructure shows large, fairly uniform grains unlike those obtained in lithium-aluminum ferrites. As a result of obtaining these preliminary good properties, the lithium-titanium series was examined more intensively.

5.1.1 Variation of Magnetic Properties with Titanium Substitution

In Fig. 19 we have shown the magnetic moments in Bohr magnetons and the Curie points in Centigrade degrees for the lithium-titanium ferrites ($\text{Li}_{0.5+0.5t}\text{Fe}_{2.5-1.5t}\text{Ti}_t\text{O}_4$). Our data for magnetic

moments were obtained by measuring the magnetization at 77° K in a field of 10 kilo Oe. The Curie points were obtained by measuring magnetization as a function of temperature in a field of 500 Oe. These data have been supplemented by those of Blasse [Ref. 10].

In Fig. 20, the magnetic losses for titanium-substituted lithium ferrites, taken at 2.85 GHz in a helical phaser, are plotted arbitrarily against the respective $4\pi M_s + \Delta H$ values. For comparison, the losses for a number of garnets are also plotted on the same figure. It is recognized that it would be desirable to plot the data as a function of the Polder-Smit criterion, [Ref. 11] $(4\pi M_s + H_a)$ where H_a is the anisotropy yield, $\frac{2K}{M_s}$.

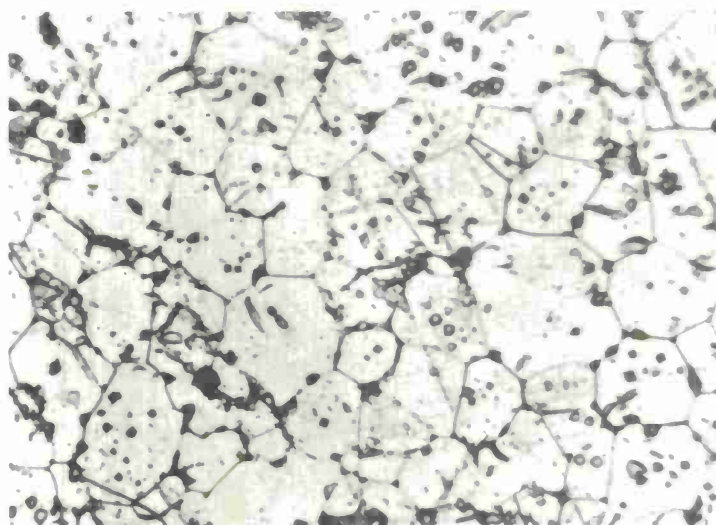


Fig. 18
 L-21-2
 1175° C - 5 Hours
 3.5 mm = 10μ
 Chemical Etch

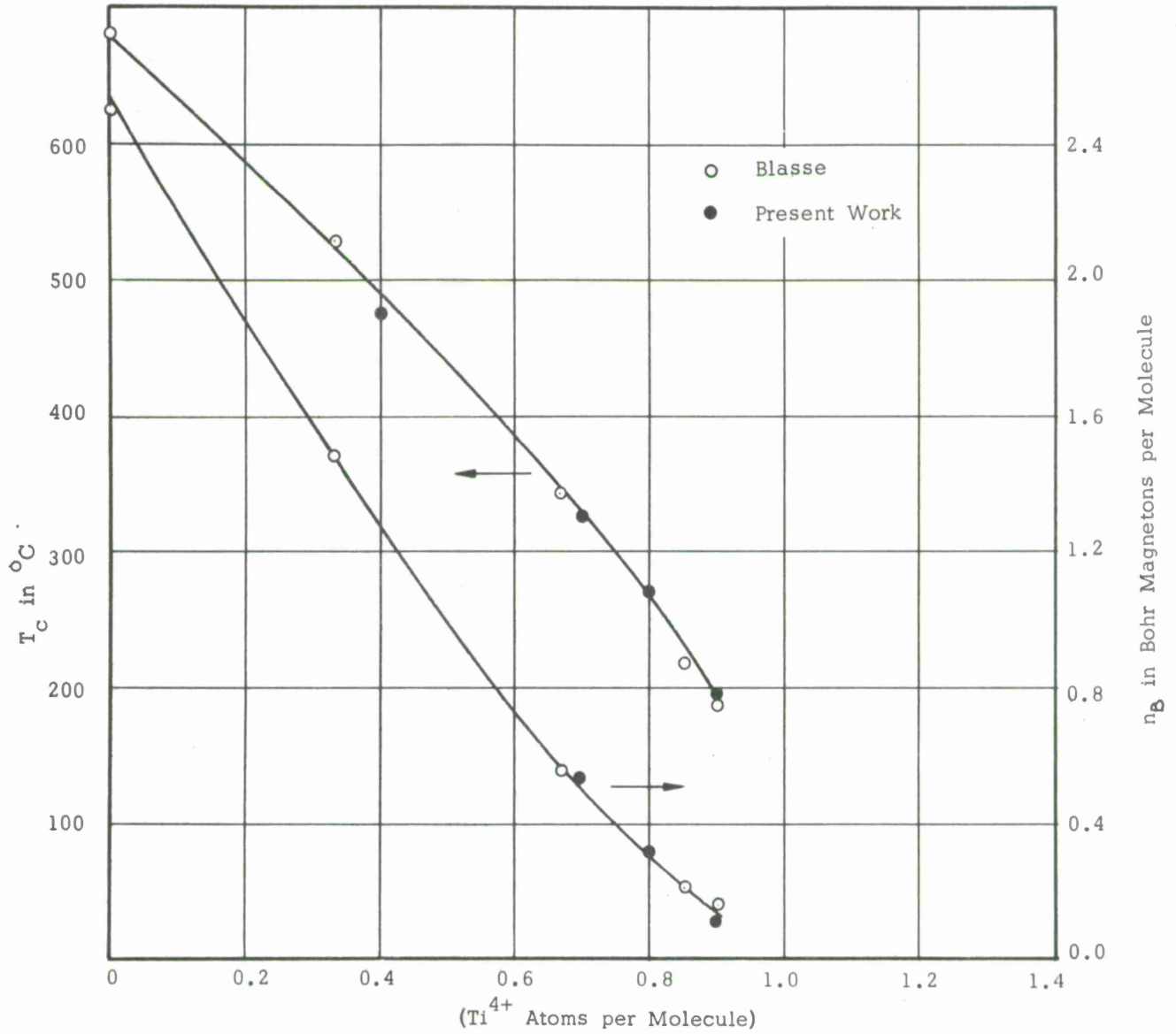


Fig. 19 Curie Point (T_c) and Magnetic Moment (n_B)
Versus Ti^{4+} Substitution

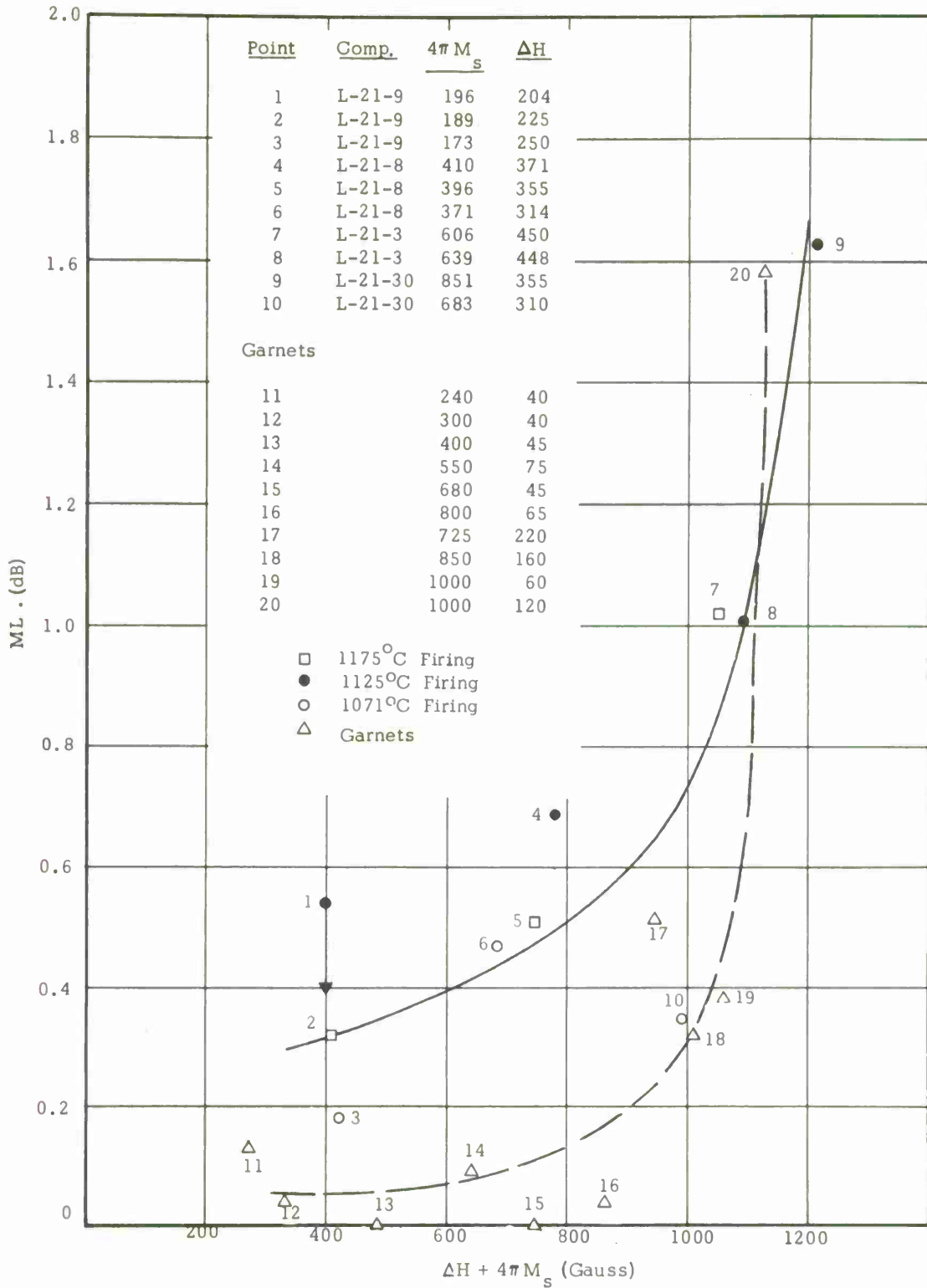


Fig. 20 Magnetic Loss for Lithium Titanium Samples

In addition to the effect from the anisotropy field, ΔH contains contributions from the intrinsic linewidth and porosity broadening. Neither of these effects is expected to be large in the data reported here. Thus, for convenience ΔH was used.

It may be noted that, in accordance with the Polder-Smit criterion [Ref. 11] for both garnets and the lithium-titanium ferrites, the losses increase sharply when $(4\pi M_s + \Delta H)$ approaches ω_r/γ , where ω_r is the resonance frequency and γ the gyromagnetic ratio. Similar behavior has also been observed by Temme [Ref. 12] in a number of ferrites. The losses at $(4\pi M_s + \Delta H)$ values below ω_r/γ are dictated by the intrinsic loss in the material.

Table X shows the important magnetic properties of the lithium-titanium ferrites as a function of firing at different temperatures.

5. 1. 2 Cobalt Substitution in Lithium-Titanium Ferrite

Although from indications in the lithium-aluminum ferrites there was reason to doubt whether low field magnetic loss can be completely controlled by controlling the magnetocrystalline anisotropy, K_1 (and through K_1 the anisotropy field H_a), attempts were made to reduce the loss in lithium-titanium ferrites by Co^{2+} substitution. It was hoped that the predominantly $-K_1$ of lithium-titanium ferrite (L-21-3) could be decreased by the $+K_1$ contribution from substituted Co^{2+} , which might reduce the resonance linewidth ΔH , and give some reduction in the magnetic loss.

In Fig. 21 we have shown the variation of ΔH and coercive force H_c in L-21-3 as a function of cobalt substitution.

Figure 21 shows the Co^{2+} is ineffective in anisotropy cancellation up to a substitution level of 0.005 atoms per formula unit. After that the predominant anisotropy is positive (due to the contribution from octahedral Co^{2+}) and results in both an increased ΔH and an increasing H_c .

Table IX. Data Obtained on Lithium-Titanium Samples

Composition Number	Firing Temp./Time (° C/Hours)	Magnetic Loss (db)	Dielectric Loss (db)	ΔH (oe)	Density (g/cc)	Porosity	$4\pi M_s$ (gauss)	B_r (gauss)	H_c (oe)	Curie Temp. (° C)
L-21-2	1175/5	>10	7.6	540	4.24	4.5%	1430	1070	2.1	468
L-21-3	1175/5	1.14	1.54	440	4.00	6.9%	593	430	2.4	347
Gd Garnet		0.65	0.42	220			725			

Table X. Data for Lithium Titanium Specimens

Sample	Firing	Density	D.L.	M.L.	ΔH	$4\pi M_s$	$\frac{B_r}{4\pi M_s}$	H_c	T_c
L-21-30	1125/5	4.24	.67	1.63	355	844	.72	5.28	330
	1071/5	3.78	.56	.35	310	683	.68	4.08	321
	1000/5	3.29	.64	.02	425	584	.59	4.5	
L-21-3	1175/5	3.94	1.04	1.02	450	606	.71	4.18	317
	1125/5	3.76	1.1	1.01	448	639	.74	2.45	327
	1000/5	3.13	.86	.33	480	517	.56	4.3	
L-21-8	1175/5	3.68	.63	.51	355	396	.60	3.0	
	1125/5	3.72	.77	.69	371	410	.66	2.87	269
	1071/5	3.55	.81	.47	314	371	.59	2.4	240
	1000/5	3.22	.86	.11	370	337	.58	4.5	
L-21-9	1175/5	3.54	.38	.32	225	189	.37	2.29	
	1125/5	3.59	.62	.54	204	196	.60	1.92	195
	1071/5	3.41	.81	.18	250	173	.39	2.72	172
	1000/5	3.12	.60	.10	258	165	.45	3.1	

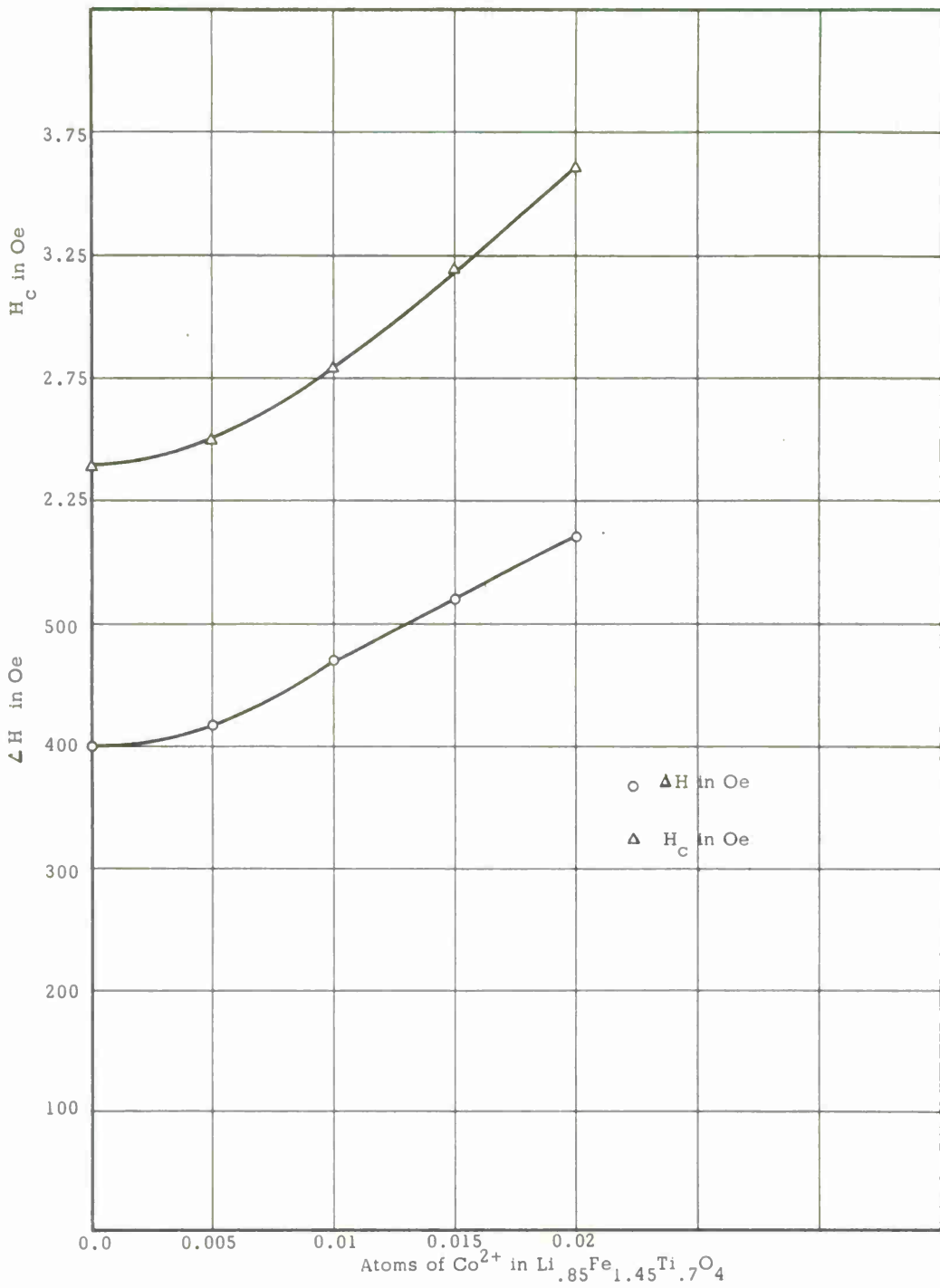


Fig. 21 H_c & ΔH vs Co^{2+} doping in $\text{Li}_{.85}\text{Fe}_{1.45}\text{Ti}_{.7}\text{O}_4$

Our own low temperature saturation magnetization measurements and the measurements reported by Blasse [Ref. 10] confirm that the titanium ions replace octahedral iron atoms by preferentially occupying the octahedral sites in lithium ferrite. This results [Ref. 13] in a decrease of the net magnetocrystalline anisotropy (K_1). It may be argued therefore that only a minute amount of Co^{2+} (i. e. , less than 0. 005 atoms per formula unit) is required to obtain anisotropy cancellation in $\text{Li}_{0.85}\text{Fe}_{1.45}\text{Ti}_{0.7}\text{O}_5$.

In Fig. 22, we have shown the observed resonance linewidth in the same lithium-titanium ferrite when Co^{2+} was added in steps of 0. 0025 atoms per formula unit to a total substitution of 0. 01 atoms per formula unit. This figure shows that Co^{2+} is definitely inactive in anisotropy cancellation in lithium-titanium ferrite.

Divalent cobalt (Co^{2+}) substitution is extensively practiced to obtain the cancellation of magnetocrystalline anisotropy in ferrites [Refs. 15-19]. In general, though, the approach has been empirical, because the contribution of positive anisotropy ($+K_1$) per atom of Co^{2+} is variable from one host ferrite to another. Furthermore, in addition to our observations above, it has been observed by others [Ref. 14] that Co^{2+} substitution can sometimes be totally ineffective in anisotropy cancellation, even though the host, a lithium-titanium ferrite, has a predominantly negative magnetocrystalline anisotropy. We therefore attempted to clarify the role of Co^{2+} in lithium ferrites with different diamagnetic substitutions and then draw some conclusions about spinels in general. These results are reported in a separate publication [Ref. 20].

5. 1. 3 Development of Low Loss Lithium-Titanium Ferrites

The data taken on the undoped lithium-titanium ferrites indicated that the losses were not sufficiently low. Furthermore, the Curie temperature

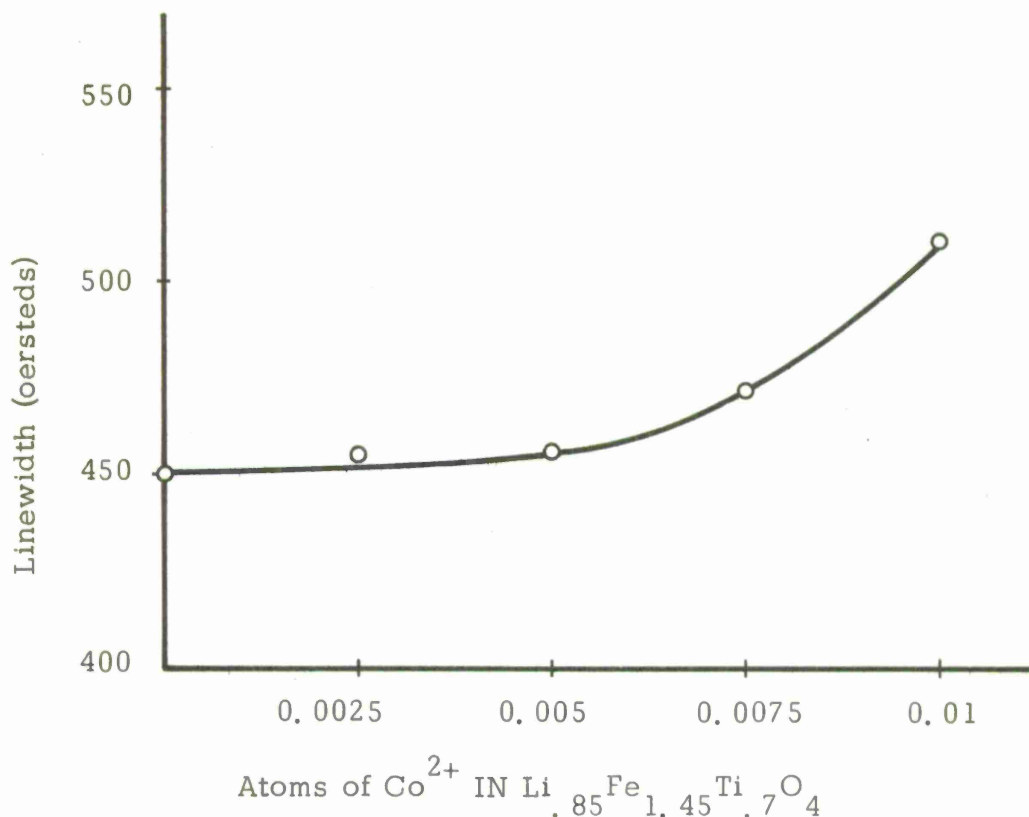


Fig. 22 Variation of Linewidth with Co²⁺ Content in L-21-3
Cobalt was Introduced in Steps of 0.0025 Atoms
per Formula Unit

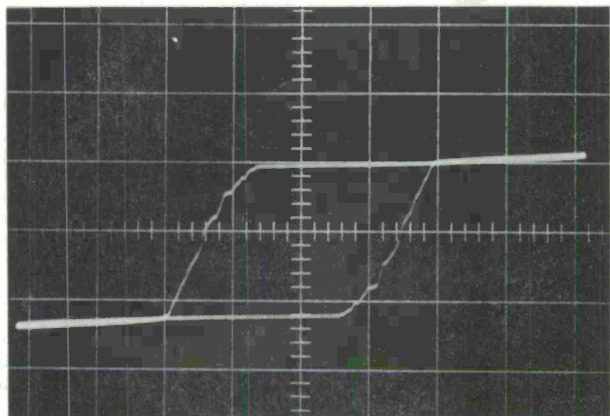
was reduced more by titanium than by aluminum. Because of the requirement of keeping the electric charge balanced while adding Ti⁴⁺, it was necessary to add extra Li⁺ atoms. Low temperature saturation magnetization and X-ray work [Ref. 10] on lithium-titanium ferrites show that the excess Li⁺ over 0.5 atoms per formula unit occupies tetrahedral sites by replacing Fe³⁺. This causes a large change in the tetrahedral-octahedral (or "A-B") superexchange resulting in a rapid decrease of the Curie point. Cu²⁺ was added to the lithium-titanium compositions to remove tetrahedral Li⁺ (one Cu²⁺ replacing half Li⁺ and half an atom of Fe³⁺).

Table XI shows the magnetic properties of copper-substituted lithium-titanium ferrites. It was suspected that the high coercive forces obtained by firing at 1175° C and 1125° C might be the result of copper volatility or second phases at elevated temperatures. Figure 23 shows hysteresis loops for L-21-31 obtained by firing toroid-shaped specimens at 1125° C, 1071° C and 1000° C respectively. The kinks in the loop observed in the 1125° C specimen vanish on firing low. The coercive force falls from 5.0 Oe to 2.88 Oe on firing at 1071° C, but increases to 4.5 Oe when fired at 1000° C. The initial decrease suggests that the kinks in the loop and the high coercive force are not intrinsic properties of copper-substituted lithium-titanium ferrites but are due to some inhomogeneities. It is interesting to note that the observation of microstructures did not reveal any evident second phase in the high temperature firing. However, firing at 1000° C decreased the grain size and increased the porosity greatly, which explains the increase in H_c and fall in remanence ratio. A study of the magnetic loss (Fig. 24) of the lithium-titanium-copper specimens shows essentially the same behavior as the garnets and the lithium-titanium ferrites. It is to be noted that Fig. 24 has a different ordinate scale compared to Fig. 20.

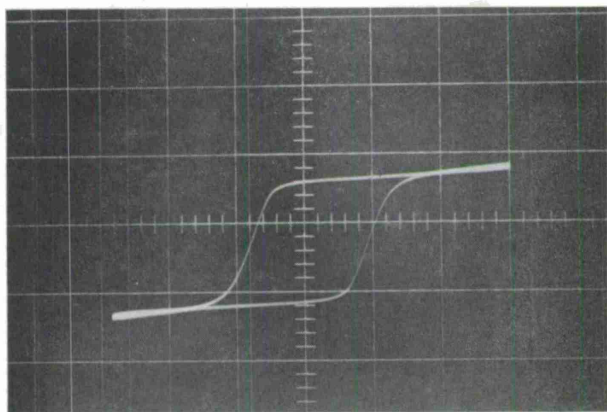
Because of specific requirements for materials with saturation magnetizations in the range of 400 to 1000 gauss, emphasis was placed on optimizing the losses, coercive forces, and remanence ratios of materials with these values of $4\pi M_s$. The copper-doped lithium-titanium ferrites were investigated from this standpoint. Small fractions of manganese were included to improve dielectric losses, and the firing conditions were altered to optimize the various properties of interest. The results for representative samples are given in Table XII and Fig. 26. In Table XII a number of compositions are listed in order of their $4\pi M_s$ values. Magnetizations from 437 to 875 gauss are represented.

Table XI. Data for Lithium Titanium Copper Specimens

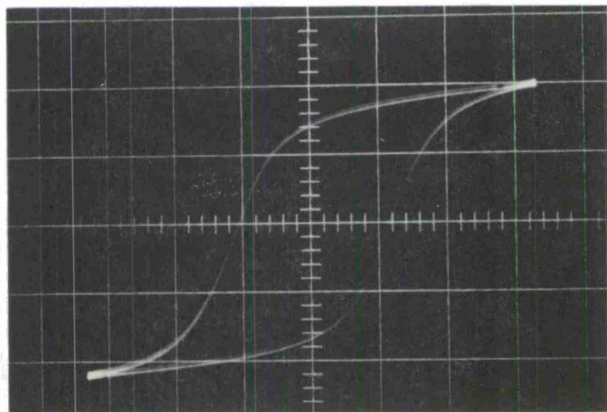
Sample	Firing	Density	D.L.	M.L.	ΔH	$4\pi M_s$	$\frac{B_r}{4\pi M_s}$	H_c	T_c
L-21-5	1175/5	3.81	.39	1.85	355	535	.76	5.51	283
	1125/5	3.78	.46	.97	364	547	.76	4.38	287
	1071/5	3.59	.52	.40	350	496	.68	2.56	289
L-21-6	1125/5	3.86	.38	.74	240	493	.65	4.91	271
	1091/5	3.66	.76	.43	265	428	.66	2.8	266
L-21-31	1125/5	3.92	.68	4.17	423	859	.72	5.0	336
	1071/5	3.51	1.55	2.22	450	736	.64	2.88	346
L-21-32	1125/5	3.81	1.68	14.04	500	883	.66	3.0	362
	1071/5	3.57	.66	16.9	513	854	.61	3.12	364
L-21-33	1125/5	4.33	.76	1.04	342	667	.43	2.5	305
	1071/5	4.15	.66	1.6	290	641	.47	2.64	299



(F352)
 1125°C Firing
 $H_c = 5.04$ oe
 $B_r = 617$ Gauss



(F360)
 1071°C Firing
 $H_c = 2.88$ oe
 $B_r = 475$ Gauss



(F370)
 1000°C Firing
 $H_c = 4.5$ oe
 $B_r = 336$ Gauss

Fig. 23. Hysteresis Loops as a Function of Firing Temperature
 Composition L-21-31

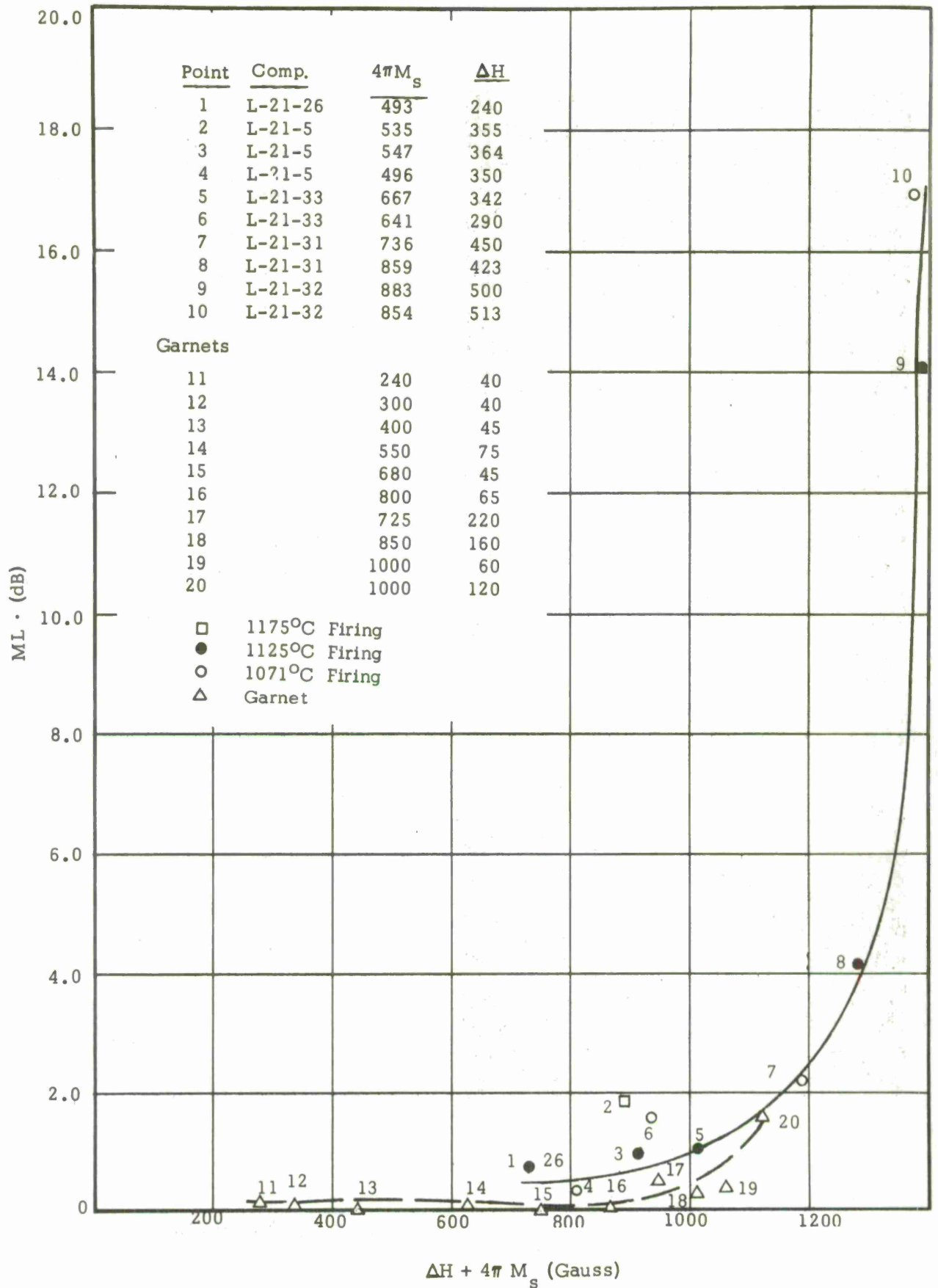


Fig. 24 Magnetic Loss for Lithium Titanium Copper Samples

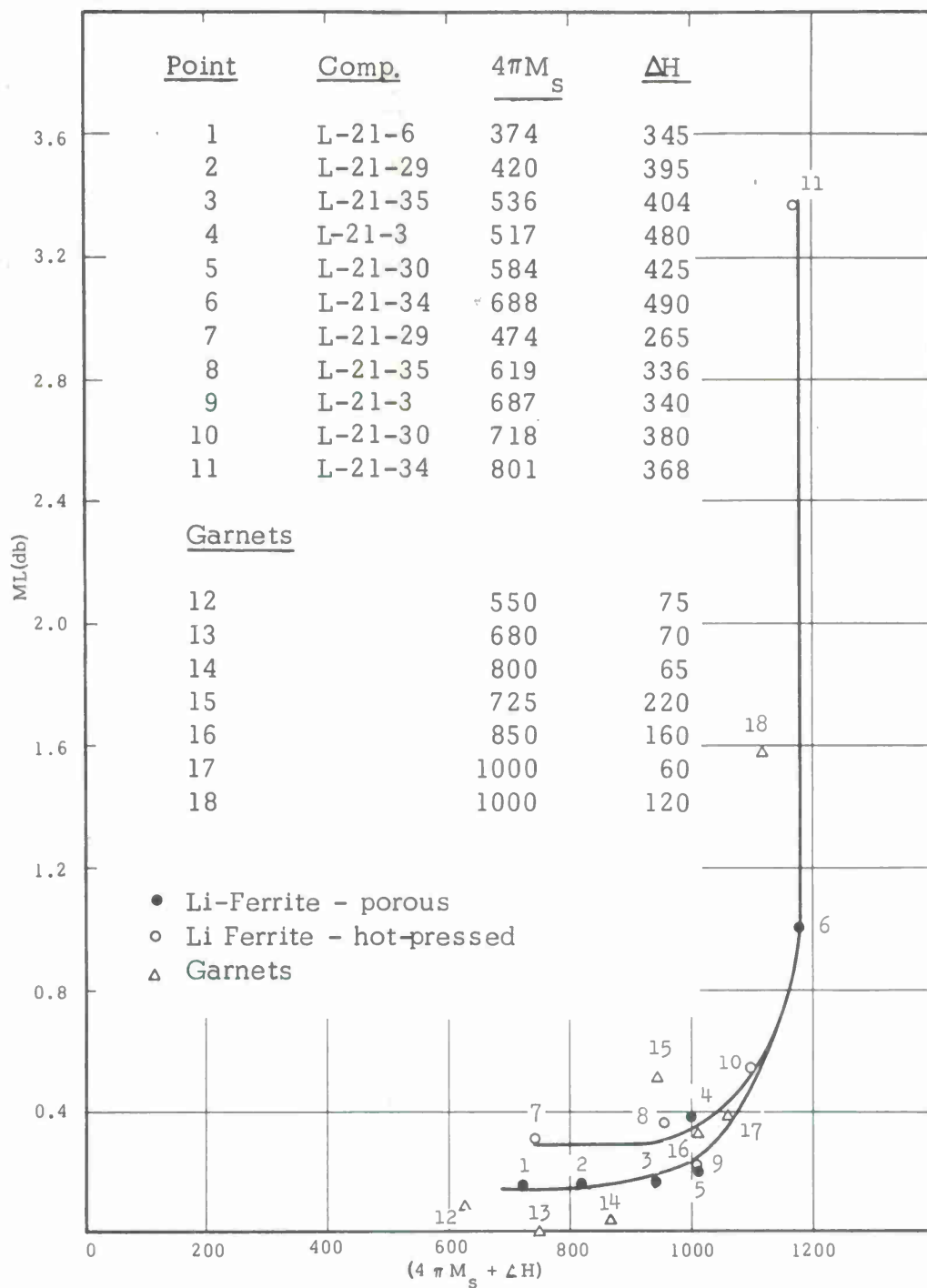


Fig. 25 Magnetic Loss for Hot-Pressed Lithium-Titanium Ferrites compared with Conventionally prepared Lithium-Titanium Ferrites and Garnets

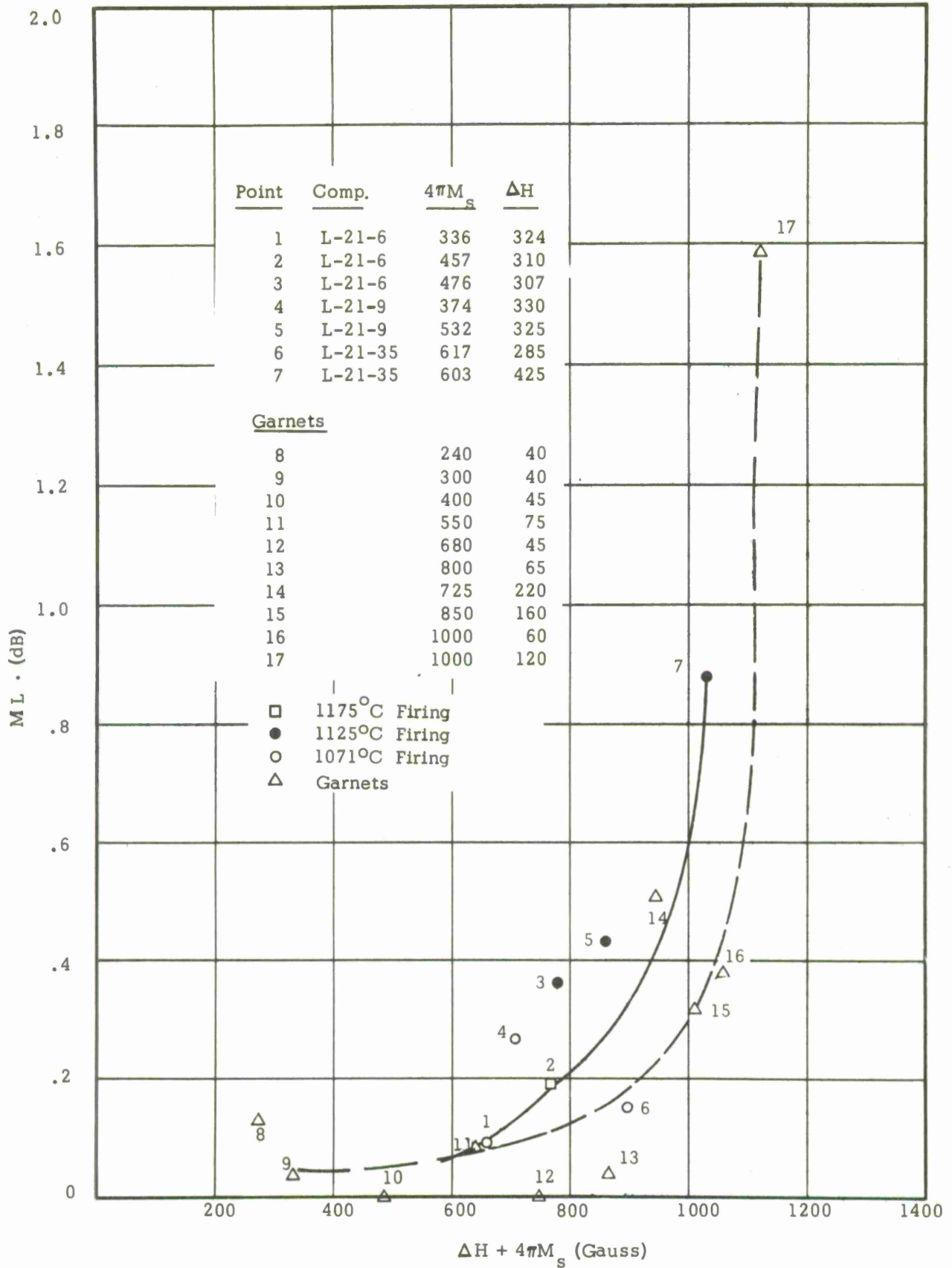


Fig. 26 Magnetic Loss for Lithium Titanium Copper Manganese Samples

Table XII. Compositions with $4\pi M_s$ from 437 to 875 Gauss

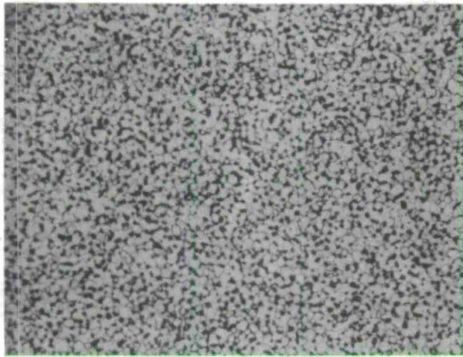
Comp No.	Firing ($^{\circ}\text{C}/\text{h}$)	Density g/cm^3	Diel. Loss (db)	Mag. Loss (db)	Linewidth (oe)	$4\pi M_s$ (Gauss)	B_r (Gauss)	$\frac{B_r}{4\pi M_s}$	H_c (oe)	T_c ($^{\circ}\text{C}$)
L-21-34	1125/5	4.10	0.58	3.48	395	875	650	0.74	4.0	336
L-21-67	1115/5	3.62	0.39	>10	492	849	590	0.69	4.4	358
L-21-35	1125/5	3.79	0.58	0.88	425	603	410	0.68	3.8	302
L-21-29	1125/5	3.68	0.47	0.43	325	532	325	0.61	2.6	254
L-21-26	1115/5	3.74	0.53	0.50	243	439	312	0.71	4.6	268
L-21-68	1115/5	3.64	0.67	<0.05	292	437	340	0.78	4.2	275
Gd Garnet			0.44	0.65	220	725				

5. 1. 4 Hot-Pressing of Lithium-Titanium Ferrites

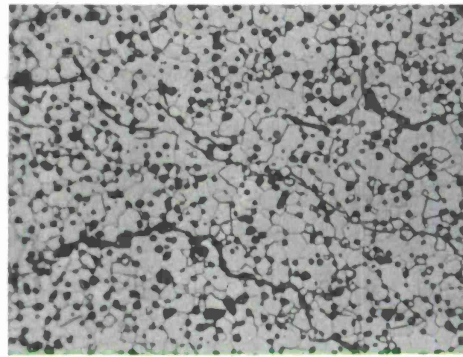
Hot-pressing of lithium-titanium ferrites was investigated in order to obtain increased densities. During the course of the program, it had been seen that the best magnetic losses were obtained when firings were conducted at low temperatures. However, such samples are porous, have a low remanence ratio and a high coercive force. If samples can be hot pressed without detrimentally affecting their magnetic loss property, the increased density might result in improvements in the other properties of interest.

Samples L-21-3, L-21-30, L-21-34, L-21-29, L-21-6, and L-21-35 were hot pressed to 1000° C for 3-1/2 hours. As expected, high density values were obtained, the $4\pi M_s$ value increased, and ferromagnetic resonance linewidth (ΔH) decreased. In Fig. 25, we have displayed the magnetic loss as a function of $(4\pi M_s + \Delta H)$, before and after hot pressing. The magnetic loss data for similar $4\pi M_s$ garnets are also shown for a comparison. It is seen that the decrease in ΔH is compensated for by the increase in $4\pi M_s$. Furthermore, the losses for low $(4\pi M_s + \Delta H)$ values seem to have risen with hot pressing

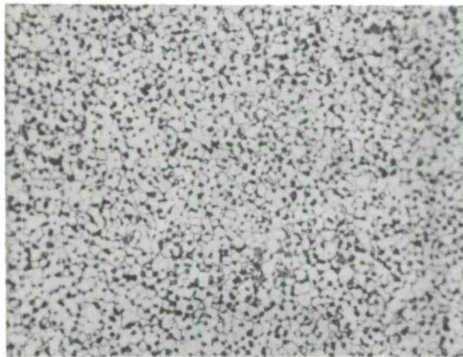
Another undesirable result of the hot pressing treatment has been an increase of coercive force to an average value of 6 Oe from an average starting value of 4 Oe. On conventionally refiring the hot pressed toroids to 1093° C, the grain size increased (see Fig. 27) but the coercive force did not change. It was at this juncture that the cracks shown in Fig. 27 became visible, and, on examination of hot pressed cylinders, it was found that microscopic cracks were present after hot pressing. These may be responsible for the observed high coercive force.



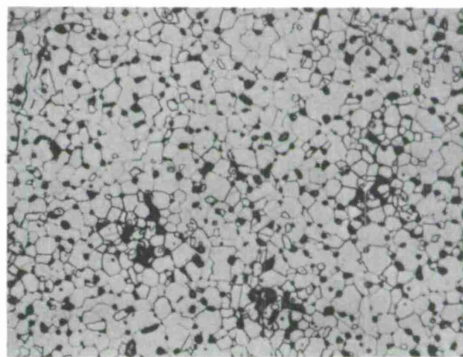
Sample #L-21-3/F613
After hot pressing at 1000°C



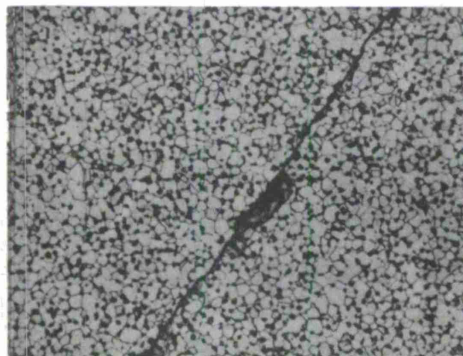
Sample #L-21-3/F643
Refired to 1093°C after
hot pressing



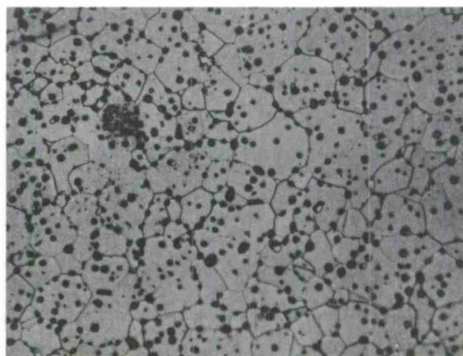
Sample #L-21-34/F616
After hot pressing at 1000°C



Sample #L-21-34/F643
Refired to 1093°C after
hot pressing



Sample #L-21-6/F615
After hot pressing at 1000°C



Sample #L-21-6/F643
Refired to 1093°C after
hot pressing

All micrographs at magnification of 195X

Fig. 27 Microstructure of hot pressed and refired samples

5. 1. 5 Fluxing Experiments

Even though hot pressing can result in a dense material it is an unattractive commercial proposition for manufacturing large batches of bars for use in array radars. Hence, we have also investigated the avenue of using fluxes to make dense materials by conventional sintering.

One approach was to use LiF instead of lithium carbonate as a starting material but this did not result in better properties and hence was abandoned.

The second and more successful approach has been to add small (e. g. 1 wt %) amounts of different fluxes like LiF, ZnO, CuO, etc., to identical batches of a 850 gauss materials. This results in good densification (95 to 100% of X-ray density by moderate temperature sintering) but there are also problems of second phases and cracks due to strong contraction at soak temperature. These problems are now being attacked.

5. 2 Conclusion

It may be concluded that the lithium-titanium materials show considerable promise for microwave applications. Their sintering properties are a significant improvement over lithium-aluminum ferrites, and their loss properties are similar to garnets of comparable $4\pi M_s$ values. Furthermore, their remanence ratios are usually greater than 0. 65 and in some cases can be made to approach 0. 80.

Although the microstructural properties compare favorably with the lithium-aluminum ferrites, there is still room for advancement in comparison with garnets. Greater densification, increased grain size, and better uniformity of grain sizes can be expected to contribute to lower coercive forces, higher remanence ratios, lower magnetic losses, and decreased linewidths.

6.0 REFERENCES

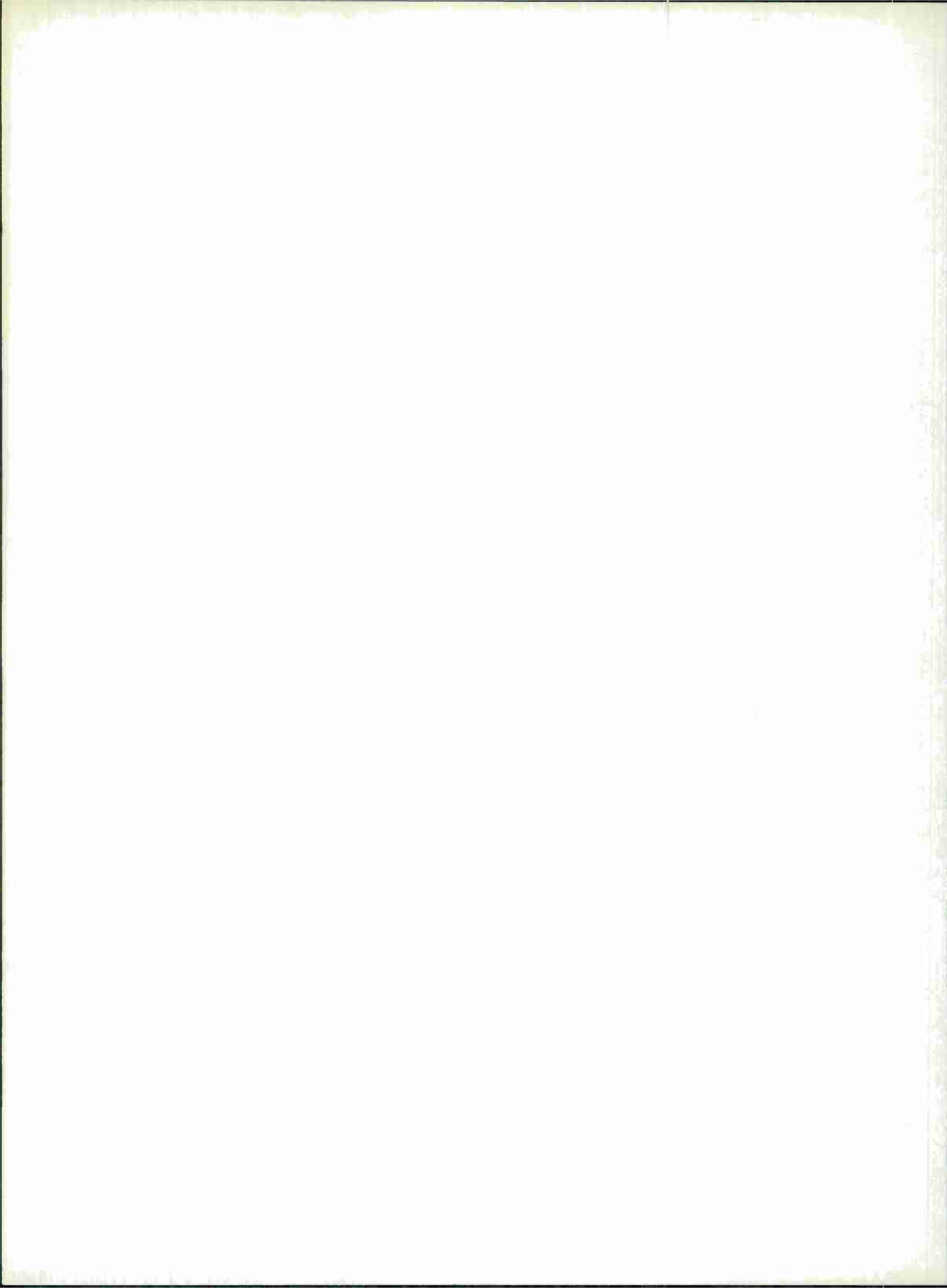
1. "Development of Helical Phase-Shifters," Final Report, Subcontract No. 250, Prime Contract No. AF19(628)-500, General Electric Company, December (1964).
2. A. S. T. M. Method, C524-63T.
3. J. A. Schulkes and G. Blasse, *J. Phys, Chem. Solids* 24, 1651-1655 (1963).
4. E. W. Gorter, Thesis, University of Leyden, 1954.
5. R. L. Comstock and J. P. Remeika, *J. Appl. Phys.* 35, 1018 (1964).
6. E. Schlomann, *A. I. E. E. (Spec. Publ.)*, T-91, 600 (1956).
7. M. H. Sirvetz and J. H. Saunders, *Phys. Rev.* 102, 366 (1956).
8. H. P. J. Wijn, E. W. Gorter, C. J. Esveldt, and P. Geldermans, *Philips Tech. Rev.* 16, 49 (1954).
9. P. D. Baba, *J. Am. Ceram. Soc.* 48, 305-309 (1965).
10. G. Blasse, *Philips Res. Rep., Suppl.* #3, p. 98 (1964).
11. D. Polder and J. Smit, *Revs. Mod. Phys.* 25, 89 (1953).
12. D. H. Temme, private communication.
13. V. J. Folen, *J. Appl. Phys.* 31, 166S (1960).
14. Final Report No. WF-2430, Contract No. NObsr 77618, Motorola Inc. (1961).

15. L. R. Bickford, J. M. Brownlow and R. F. Penoyer, Proc. IEE 3104, 238 (1957).
16. M. A. Stel'mashenko, Soviet Phys. Solid State 9, 1137 (1967).
17. J. E. Pippin and C. L. Hogan, Trans. IRE-MTT 6, 77 (1958).
18. M. H. Sirvetz and J. H. Saunders, Phys. Rev. 102, 366 (1956).
19. R. F. Pearson, Proc. Phys. Soc. (London) 74, 505 (1959).
20. S. K. Banerjee, P. D. Baba, B. J. Evans, and S. S. Hafner, to be published.

DOCUMENT CONTROL DATA - R&D

(Security classification of title, body of abstract and indexing annotation must be entered when the overall report is classified)

1. ORIGINATING ACTIVITY (Corporate author) AMPEX Corporation under Purchase Order No. CC-807 to M. I. T. Lincoln Laboratory		2a. REPORT SECURITY CLASSIFICATION Unclassified	
		2b. GROUP None	
3. REPORT TITLE Microwave Ferrite Program			
4. DESCRIPTIVE NOTES (Type of report and inclusive dates) Summary Technical Report Period Ending 31 July 1968			
5. AUTHOR(S) (Last name, first name, initial) Baba, Paul D. and Banerjee, S.K.			
6. REPORT DATE Period Ending 31 July 1968		7a. TOTAL NO. OF PAGES 64	7b. NO. OF REFS 20
8a. CONTRACT OR GRANT NO. AF 19(628)-5167		9a. ORIGINATOR'S REPORT NUMBER(S) RR 68-21	
b. PROJECT NO. ARPA Order 498		9b. OTHER REPORT NO(S) (Any other numbers that may be assigned this report) ESD-TR-68-251	
c.			
d.			
10. AVAILABILITY/LIMITATION NOTICES This document has been approved for public release and sale; its distribution is unlimited.			
11. SUPPLEMENTARY NOTES None		12. SPONSORING MILITARY ACTIVITY Advanced Research Projects Agency, Department of Defense	
13. ABSTRACT A program is described in which the objective was the development of a series of lithium ferrites for latching microwave device applications. Two families of compositions were explored: lithium-aluminum ferrites and lithium-titanium ferrites. Microwave, hysteresis loop, and microstructural properties were investigated as functions of compositions and processing parameters. The lithium-titanium ferrites were found to have better sintering performance relative to the lithium-aluminum ferrites, and are considered promising materials for the intended microwave applications.			
14. KEY WORDS microwave equipment microwave ferrites microwave applications microwave materials lithium ferrites			



AMPEX

